Eur. Phys. J. C (2026) 86:16
https://doi.org/10.1140/epjc/s10052-025-15214-6

THE EUROPEAN PHYSICAL JOURNAL C

Regular Article - Theoretical Physics

Modeling theoretical charged compact stellar structures under zero complexity factor constraint in Einstein's gravity scenario

Tayyab Naseer[1,2,a], **M. Sharif**[1,b], **Javeria Javid**[1,c], **Omer A. Magzoub**[3,d], **M. Abdalla**[4,e]

[1] Department of Mathematics and Statistics, The University of Lahore, 1-KM Defence Road, Lahore 54000, Pakistan
[2] Research Center of Astrophysics and Cosmology, Khazar University, 41 Mehseti Street, AZ1096 Baku, Azerbaijan
[3] Department of Physics, College of Sciences, University of Bisha, Bisha 61922, Saudi Arabia
[4] Department of Mathematics, College of Sciences, King Khalid University, P.O. Box 9004, Abha 61413, Saudi Arabia

Received: 30 October 2025 / Accepted: 12 December 2025

Abstract This study applies the concept of a complexity factor, originally formulated for static spherically symmetric spacetimes, to a system containing a charged fluid. The analysis commences by formulating the Einstein field equations for the anisotropic fluid and subsequently evaluating two distinct mass functions. The scalar Y_{TF} is selected as the complexity factor under Herrera's formalism due to the incorporation of the key factors for dynamical complexity, which are pressure anisotropy and energy density inhomogeneity. Furthermore, the field equations are solved by imposing several constraints, one of them being the requirement of vanishing complexity. Using two different expressions for the radial metric potential, we obtain two independent solutions. We then determine the unknowns in these models by applying the junction conditions with the Reissner–Nordström metric as the exterior spacetime. Multiple stellar candidates' observational data is assumed to check the acceptability of the obtained solutions graphically. It is concluded that both the suggested models depict stable and physically viable fluid configurations. These findings ultimately show that how well the vanishing complexity requirement behave in achieving feasible charged anisotropic fluid solutions.

1 Introduction

Most people accept that the general theory of relativity (GR) as the most trustworthy framework in the scientific world for understanding gravitational events. According to Einstein's 1915 theory, gravity is a geometric phenomenon that results from the curvature that matter and energy impose on spacetime rather than a force. The theoretical base of this relationship is provided by his field equations, connecting the energy-momentum tensor (EMT), which depicts the density and disbursement of matter and energy, to the Einstein tensor, which characterizes spacetime geometry. These equations are only tractable for accurate solutions in a restricted number of physical scenarios because of their highly non-linear nature. Analytical and numerical methods are the two main strategies used to solve this system of non-linear equations. A basic prerequisite for numerical methods is the establishment of boundary conditions. In-depth understanding of the local physical processes involved in a system is also necessary for the successful modeling. Knowledge of the dynamic interactions and physical characteristics found in the particular spacetime region under investigation is also a major part of this. Numerous physical phenomena that may be related to the isotropy and anisotropy of local pressure have been discovered [1–3]. Additionally, research has shown that the state of isotropic pressure is intrinsically unstable, impacted by variables such as dissipation, shear stresses, and uneven energy density [4].

The field equations for a static anisotropic sphere consist of three differential equations and five unknown functions pertaining to matter and metric potentials, forming an underdetermined system. In order to solve this system for a unique solution, two more constraints must be added. These constraints are frequently experimentally supported hypotheses, such as an equation of state or other physical conditions that have been verified in earlier research [5,6]. A polytropic equation of state is frequently used by researchers to examine the physical characteristics of objects that resem-

[a] e-mail: tayyabnaseer48@yahoo.com (corresponding author)
[b] e-mail: msharif.math@pu.edu.pk
[c] e-mail: javeriajavid3@gmail.com (corresponding author)
[d] e-mail: oammali@ub.edu.sa
[e] e-mail: moabdalla@kku.edu.sa

Published online: 08 January 2026

ble white dwarfs [7–9]. Anisotropic spherical configurations have been thoroughly studied within the context of GR [10–14]. However, certain techniques, such the Karmarkar condition, which builds the entire solution from a single, freely selected function, have been used to confirm their existence [15–19]. Another prerequisite for this method is conformally flat spacetime, which is defined by a vanishing Weyl tensor [20]. This demonstrates how researchers can describe the evolutionary behavior of self-gravitating entities using a variety of accessible restrictions.

Early research on self-gravitating spherically symmetric systems was predicated on an ideal fluid model, which assumes isotropic pressure. These fluids must have anisotropic internal properties due to a variety of physical considerations, as established by Jeans' work [21]. The extreme densities found in compact star objects (more than 10^{15} g/cm^3) can result in a divergence between radial and tangential pressures, according to Ruderman [22]. Anisotropic pressure, which is characterized by varying radial and transverse pressure values, is a state that compact stars under severe density develop, according to Canuto [23]. Anisotropic characteristics in compact stellar objects can be caused by a number of physical processes, including strong magnetic fields [24–27], pion condensation [28], nuclear interactions [23], the presence of a superfluid core [29], and a few others. For stability, Bowers and Liang [30] discovered that the star center's pressure anisotropy must be zero. The mass, hydrostatic equilibrium, and surface redshift of a star are all significantly influenced by this parameter. By employing pressure anisotropies and defined radial metric functions, Sharif and Naseer [31] produced anisotropic solutions and showed that the resulting models meet all relevant physical constraints. Govender, Das and their colleagues have developed multiple physically acceptable models coupled with the anisotropic fluid distribution in different theoretical frameworks [32–44].

In astronomy, complexity analysis has been a basic and popular notion for examining the structure of stars and galaxies. In order to characterize the complicated internal dynamics of astronomical objects, this complexity analysis integrates important physical factors, such as density, pressure, and heat flux. These physical factors interact dynamically to determine the complex behavior and structure of celestial objects, which together determine their evolution. For a long time, researchers from multiple kinds of professions have attempted to statistically quantify this idea by connecting it to observable facts. As discussed in [45–47], early ideas of complexity were varied and frequently conflicting, with many academics associating it with information content or thermodynamic entropy. Two disparate systems – a disordered ideal gas and a perfectly ordered crystal – were used to test the methodology in order to initially validate it. Assigning zero complexity to both extremes revealed a fundamental weakness in the initial measures and served as a major catalyst for later developments in complexity's definition.

A novel model for measuring complexity in physical systems was established by Herrera [48], who described it as a function of pressure anisotropy and density inhomogeneity. A complete set of structural scalars was obtained by him by applying an orthogonal decomposition to the curvature tensor [49,50]. For static spherically symmetric systems, the study found that the combined contributions of inhomogeneous density and pressure anisotropy constitute a crucial structural parameter known as the complexity factor. This paradigm is based on the idea that there are two different situations in which minimal complexity occurs: either a system that is absolutely homogenous and isotropic, or one in which anisotropic pressures and density inhomogeneities precisely balance one another. Since then, this method has been modified for broader uses, such as axially symmetric and time-evolving models [51,52]. Due to these advancements, in-depth research on various evolutionary routes has been done, revealing the complex physics and internal behavior of these systems [53,54]. In addition to improving complexity analysis, this thorough approach offers a strong foundation for examining the underlying mechanisms governing intricate spacetime structures and astrophysical phenomena.

A large body of literature exists that analyzed stellar objects under the vanishing complexity condition. Maurya et al. [55] employed an extended geometric deformation method alongside vanishing complexity and isotropization constraints to derive relativistic models embedded in class-I spacetimes, yielding isotropic stellar profiles that align with observed pulsars while emphasizing deformation-driven equilibrium. Building on this, Das et al. [56] introduced a novel anisotropic compact model tailored to pulsar data, using the zero-complexity condition to generate exact solutions that satisfy stability via the Tolman–Oppenheimer–Volkoff equation and causality limits. Similarly, Das and his colleagues [57] explored compact stars under Vaidya–Tikekar geometry with enforced vanishing complexity, demonstrating enhanced mass predictions and dynamical stability through adiabatic indices. In a related study, Rej et al. [58] integrated dark energy into Finch-Skea ansatz with zero complexity, predicting neutron star masses exceeding the conventional solar mass threshold, thus probing exotic matter influences on compactness. Das et al. [59] further characterized complexity in anisotropic fluids by solving Einstein's equations for spherically symmetric structures, highlighting how trace-free scalars govern pressure gradients and energy distributions. Extending to dynamical regimes, Das and his collaborators [60] examined vanishing complexity's role in self-gravitating dissipative spheres, revealing counterbalancing effects between inhomogeneity and shear on evolutionary paths. Complementary efforts by Pal et al. [61] analyzed stellar equilibrium under modified

complexity metrics, incorporating radial dependencies to refine boundary matching for realistic interiors. Finally, Das et al. [62] constructed zero-complexity anisotropic models that underscore the interplay of Weyl curvature and matter stress, validating them against pulsar observations for causal and stable profiles.

Different evolutionary routes in celestial bodies can be more effectively analyzed when electric charge is included. An electromagnetic field within a compact star can produce a repulsive force that counteracts the inward gravitational collapse of the star. As a result, compared to uncharged stars, the system has longer stability and is more adaptable. The effects of electric charge on Einstein field equations' solutions are a well-established subject of study, as examined in [63–66]. Sunzu et al. [67] investigated how charge affected the final configuration of a dense star and established a mass to radius relationship. The impact of an electromagnetic field on the characteristics and dynamics of a known spherically symmetric system was examined by Murad [68]. Using gravitational decoupling, Sharif and Sadiq [69] developed anisotropic charged solutions and specified their stable parameter ranges.

In order to investigate charged matter configurations, this work expands the current definition for anisotropic spherical systems [48] to incorporate electromagnetic effects. The structure of the paper is as follows. The Einstein–Maxwell field equations governing a static spherically symmetric anisotropic interior are presented in Sect. 2, after which the mass function is evaluated. Through the orthogonal decomposition of the curvature tensor, the structural scalars are formulated in Sect. 3, establishing the complexity factor for this system as Y_{TF}. The essential physical requirements that successful stellar models must meet are outlined in Sect. 4. Two distinct stellar solutions are developed in Sect. 5, where the unknown parameters are ascertained by applying junction conditions. A graphical analysis is also conducted by applying the results to five distinct pulsars. The final section of our study provides a summary of the key findings.

2 Einstein–Maxwell field equations

Here, the Einstein–Maxwell field equations for a spherically symmetric static system are constructed. We start with the line element to explain the geometry of spacetime inside a stellar body. To simulate the behavior of matter and energy in self-gravitating systems, this geometry must be defined precisely. Using a static spherical structure has the significant benefit of reducing the field equations' complexity. A deeper and more effective analysis of the system is made possible by this geometric assumption, which reduces the mathematical complexity of the governing equations. Our analysis commences with a spacetime interior characterized by the following line element

$$ds^2 = e^{\chi}dt^2 - e^{\lambda}dr^2 - r^2\left(d\theta^2 + \sin^2\theta d\phi^2\right), \tag{1}$$

where $\chi = \chi(r)$ and $\lambda = \lambda(r)$. The field equations, derived from the variation of the action, are given as follows

$$G_{\epsilon\sigma} = \kappa\left(T_{\epsilon\sigma} + E_{\epsilon\sigma}\right), \tag{2}$$

where $G_{\epsilon\sigma}$ is the Einstein tensor, and $T_{\epsilon\sigma}$ and $E_{\epsilon\sigma}$ are the EMTs for matter and the electromagnetic field, respectively. The coupling constant κ is assumed to be unity here.

The pressure in isotropic fluids is constant in all directions, whereas the pressure components in anisotropic fluids are directionally dependent. In relativistic astrophysics, the extreme gravitational fields and fast rotations of compact objects produce shear stresses and anisotropic pressures, making the analysis of such anisotropic systems crucial. By incorporating directionally dependent properties, the corresponding EMT yields a more faithful representation of energy and momentum distributions in high-energy regimes. Its purpose is to extend the isotropic perfect fluid framework, enabling the inclusion of greater astrophysical realism. The anisotropic fluid is characterized by an EMT of the form

$$T_{\epsilon\sigma} = (\rho + p_t)y_\epsilon y_\sigma + p_t g_{\epsilon\sigma} + (p_r - p_t)z_\epsilon z_\sigma, \tag{3}$$

the terms ρ, p_r, p_t, z_σ, and y_σ correspond to the energy density, radial pressure, tangential pressure, four-vector, and four-velocity, respectively. The last two terms are mathematically defined under the line element (1) as

$$G_\sigma = (0, -e^{\frac{\lambda}{2}}, 0, 0), \quad D_\sigma = (e^{\frac{\chi}{2}}, 0, 0, 0), \tag{4}$$

obeying the following relations $y^\sigma z_\sigma = 0$, $y^\sigma y_\sigma = 1$ and $z^\sigma z_\sigma = -1$.

The electromagnetic field is fully characterized by its EMT, expressed as

$$E_{\epsilon\sigma} = -\frac{1}{4\pi}\left[\frac{1}{4}g_{\epsilon\sigma}N^{\xi\vartheta}N_{\xi\vartheta} - N^{\vartheta}_{\epsilon}N_{\sigma\vartheta}\right], \tag{5}$$

where $N_{\xi\vartheta} = \Theta_{\vartheta;\xi} - \Theta_{\xi;\vartheta}$ is the Maxwell field tensor, and $\Theta_\vartheta = \Theta(r)\delta^0_\vartheta$ is the four-potential. The tensorial form of the Maxwell equations is as follows

$$N^{\xi\vartheta}_{;\vartheta} = 4\pi\jmath^{\xi}, \quad N_{[\xi\vartheta;\epsilon]} = 0,$$

where the current and charge densities are denoted by $\jmath^{\xi}$ and γ, respectively, and $\jmath^{\xi} = \gamma y^{\xi}$. In this scenario, the above (left) equation becomes

$$\chi'' + \frac{1}{2r}\left\{4 - r(\chi' + \lambda')\right\}\chi' = 4\pi\gamma e^{\frac{\chi}{2}+\lambda}, \tag{6}$$

where $' = \frac{d}{dr}$. When the above expression is integrated, the outcome is

$$\chi' = \frac{q}{r^2} e^{\frac{\chi+\lambda}{2}}, \quad q = \int_0^r \gamma e^{\frac{\lambda}{2}} \bar{r}^2 d\bar{r}, \tag{7}$$

where the total charge present in the spherical configuration denoted by Eq. (1) is represented by $q = q(r)$.

For the spherical metric (1), the non-zero components of the Einstein field equations (2) are derived as follows

$$\rho + \frac{q^2}{r^4} = \frac{1}{r^2} - e^{-\lambda}\left(\frac{1}{r^2} - \frac{\lambda'}{r}\right), \tag{8}$$

$$p_r - \frac{q^2}{r^4} = e^{-\lambda}\left(\frac{1}{r^2} + \frac{\chi'}{r}\right) - \frac{1}{r^2}, \tag{9}$$

$$p_t + \frac{q^2}{r^4} = \frac{e^{-\lambda}}{4}\left(\chi'^2 - \chi'\lambda' + 2\chi'' - \frac{2\lambda'}{r} + \frac{2\chi'}{r}\right). \tag{10}$$

The Tolman–Oppenheimer–Volkoff (TOV) equation, which regulates the equilibrium between strong gravitational fields and internal pressure, describes the structure of ultra-dense compact stars in Einstein's theory. The relativistic effects that become predominant in massively compact objects are incorporated into this framework, which expands on the traditional idea of hydrostatic equilibrium, where pressure gradients resist gravitational collapse. The conservation law, which may be written as $\nabla_\epsilon(T^{\epsilon\sigma} + E^{\epsilon\sigma}) = 0$, yields this condition, which reduces to [70,71]

$$\frac{dp_r}{dr} + \frac{\chi'}{2}(\rho + p_r) - \frac{2}{r}(p_t - p_r) - \frac{2qq'}{r^4} = 0. \tag{11}$$

The active gravitational energy inside a spherical border is measured by the Misner–Sharp mass function, which is an important parameter in gravitational collapse research. The Misner–Sharp formulation, in contrast to prior mass definitions, simultaneously takes the enclosed matter and its associated gravitational curvature by incorporating the spacetime metric. For the analysis of cosmic horizons and star collapse, this renders it indispensable. The primary benefit is that it may simplify intricate gravitational dynamics into a single, physically significant, and tractable quantity, generating testable predictions for extremely curved spacetimes. The following form expresses the fundamental relationship as [72]

$$m(r) = \frac{r}{2}\left(1 - e^{-\lambda} + \frac{q^2}{r^2}\right). \tag{12}$$

This can be expressed differently using the energy density found in Eq. (8) as

$$m(r) = \frac{1}{2}\int_0^r \rho \bar{r}^2 d\bar{r} + \int_0^r \frac{qq'}{r} d\bar{r}. \tag{13}$$

For χ', Eq. (9) gives an expression using the mass (12) as

$$\chi' = \frac{p_r r^4 - 2q^2 + 2mr}{r(r^2 + q^2 - 2mr)}. \tag{14}$$

Inserting this result into Eq. (11) produces the following form

$$\frac{dp_r}{dr} + \frac{p_r r^4 - 2q^2 + 2mr}{2r(r^2 + q^2 - 2mr)}(\rho + p_r) + \frac{2\Pi}{r} - \frac{2qq'}{r^4} = 0, \tag{15}$$

where $\Pi = p_r - p_t$ quantifies the pressure anisotropy.

3 Formulation of structure scalars via orthogonal splitting

An essential component of contemporary research on gravitationally bound astrophysical systems is the evaluation of structural complexity. Although the term "complexity" has been defined in a variety of methods across the literature, a fundamental viewpoint is that total homogeneity and isotropy within a system define no complexity. In this model, the complexity factor functions as a scalar metric that encodes the pressure anisotropy and density contrasts of the system. A fundamental concept of complexity based on these two characteristics was first proposed by Herrera [48]. He identified the complexity factor as one of the scalar functions resulted from the orthogonally decomposed Riemann tensor [49,50]. The computational framework for the complexity factor is briefly summarized here, along with its correlations to important physical parameters. The Riemann curvature tensor admits a decomposition into trace and trace-free components, mathematically represented as

$$R^{\eta\zeta}_{\epsilon\vartheta} = C^{\eta\zeta}_{\epsilon\vartheta} + 2\left(T^{[\eta}_{[\epsilon}\varphi^{\zeta]}_{\vartheta]} + E^{[\eta}_{[\epsilon}\varphi^{\zeta]}_{\vartheta]}\right) + T\left(\frac{1}{3}\varphi^{\eta}_{[\epsilon}\varphi^{\zeta}_{\vartheta]} - \varphi^{[\eta}_{[\epsilon}\varphi^{\zeta]}_{\vartheta]}\right), \tag{16}$$

where $X_{\eta\epsilon}$ and $Y_{\eta\epsilon}$ are the tensors provided by

$$Y_{\eta\epsilon} = \mathcal{R}_{\eta\zeta\epsilon\vartheta} y^\zeta y^\vartheta, \tag{17}$$

$$X_{\eta\epsilon} = {}^*\mathcal{R}^*_{\eta\zeta\epsilon\vartheta} y^\zeta y^\vartheta = \frac{1}{2}\lambda^{\alpha\beta}_{\eta\zeta}\mathcal{R}^*_{\alpha\beta\epsilon\vartheta} y^\zeta y^\vartheta, \tag{18}$$

where $\lambda^{\alpha\beta}_{\eta\zeta}$ is the Levi-Civita symbols and $\mathcal{R}^*_{\eta\zeta\epsilon\vartheta} = \frac{1}{2}\lambda_{\alpha\beta\epsilon\vartheta}\mathcal{R}^{\alpha\beta}_{\eta\zeta}$. The trace ($Y_T$, X_T) and trace-free (Y_{TF}, X_{TF}) components of these tensors can be decomposed as follows

$$Y_{\eta\epsilon} = \frac{h_{\eta\epsilon} Y_T}{3} + \left(z_\eta z_\epsilon + \frac{h_{\eta\epsilon}}{3}\right) Y_{TF}, \tag{19}$$

$$X_{\eta\epsilon} = \frac{h_{\eta\epsilon} X_T}{3} + \left(z_\eta z_\epsilon + \frac{h_{\eta\epsilon}}{3}\right) X_{TF}. \tag{20}$$

Here, $h_{\eta\epsilon} = g_{\eta\epsilon} - y_\eta y_\epsilon$ is the projection tensor. The following scalar quantities are obtained using Eqs. (16)–(20) in a sequence of uncomplicated algebraic manipulation as

$$X_T = \rho + \frac{q^2}{r^4}, \tag{21}$$

$$X_{TF} = \frac{\Pi}{2} - \mathcal{B} + \frac{q^2}{r^4}, \tag{22}$$

$$Y_T = \frac{1}{2}(\rho + 3p_r - 2\Pi) + \frac{q^2}{r^4}, \tag{23}$$

$$Y_{TF} = \frac{\Pi}{2} + \mathcal{B} + \frac{q^2}{r^4}, \tag{24}$$

with the electric Weyl scalar $\mathcal{B}$, expressed as

$$\mathcal{B} = -\frac{e^{-\lambda}}{4}\left[\chi'' + \frac{\chi'^2 - \lambda'\chi'}{2} - \frac{\chi' - \lambda'}{r} + \frac{2(1-e^{\lambda})}{r^2}\right]. \tag{25}$$

The degree of local pressure anisotropy and the inhomogeneity of the energy density of a self-gravitating system are described by the scalar functions (21)–(24). Therefore, the challenge is to identify the complexity factor among these four scalars. We determine that the scalar Y_{TF} is the complexity factor since it is the just quantity that includes all of the crucial parameters. The following expression, which is produced by substituting Eqs. (8), (24), and (25) confirms this, given by

$$Y_{TF} = \frac{3q^2}{2r^4} - \frac{1}{2r^3}\int_0^r \bar{r}^3\rho' d\bar{r} + \Pi, \tag{26}$$

where we notice that, for an isotropic, uniform, and uncharged fluid distribution, this scalar vanishes.

A framework to quantify how a system's total energy, momentum, and stress all work together to determine its gravitational field is provided by the Tolman mass idea. In this way, it deepens our knowledge of cosmic structure by providing a means of investigating the complex relationship between matter and spacetime geometry. This quantity is defined as [73]

$$m_T = \frac{1}{2}\int_0^r \bar{r}^2 e^{(\chi+\mu)/2}(T_0^0 + E_0^0 - T_1^1 - E_1^1 - 2T_2^2 - 2E_2^2)d\bar{r}, \tag{27}$$

which, upon substitution of Eq. (26), becomes

$$m_T = (m_T)_\Sigma\left(\frac{r}{R}\right)^3 + 2r^3\int_r^R \frac{q^2 e^{(\chi+\lambda)/2}}{\bar{r}^5}d\bar{r} + r^3\int_r^R \frac{e^{(\chi+\lambda)/2}}{\bar{r}}\left\{\Pi - \frac{1}{2r^3}\int_0^r \bar{r}^3\rho' d\bar{r} - \frac{q^2}{2r^4}\right\}d\bar{r}. \tag{28}$$

In terms of the scalar (26), this is expressed as

$$m_T = (m_T)_\Sigma\left(\frac{r}{R}\right)^3 + r^3\int_r^R \frac{1}{\bar{r}}e^{(\chi+\lambda)/2}\left(Y_{TF} + \frac{2q^2}{\bar{r}^4}\right)d\bar{r}. \tag{29}$$

Equation (29) reveals that the Tolman mass is determined by the anisotropy and density inhomogeneity, as quantified by the complexity factor Y_{TF}.

It is important to recognize that a state of zero complexity is not exclusive to systems with homogeneous density and isotropic pressure. Equation (26) indicates that Y_{TF} vanishes only under the following specific condition

$$\Pi = \frac{1}{2r^3}\int_0^r \bar{r}^3\rho' d\bar{r} - \frac{3q^2}{2r^4}. \tag{30}$$

Substituting the expressions for ρ, p_r, and p_t from Eqs. (8)–(10) yields

$$22q^2 e^{\lambda(r)} + r^3\left(\chi'(r)\left(r\lambda'(r) - r\chi'(r) + 2\right) - 2r\chi''(r)\right) = 0. \tag{31}$$

The system of field equations comprises five unknown functions, such as λ, χ, ρ, p_r, and p_t. Equation (31) now provides a fourth independent relation, which will be solved in conjunction with a specified form for the radial metric function to determine a unique solution in the subsequent analysis. The condition (30) acts as an effective non-local equation of state, greatly enabling the derivation of solutions to the field equations.

4 Physical existence criteria of realistic celestial models

The scientific literature presents numerous methodologies for obtaining solutions to the gravitational field equations that model physically admissible compact stellar objects. Solutions that fail to meet the required physical acceptability criteria cannot be considered viable models for real astrophysical objects. Various researchers have compiled a set of physical acceptability conditions essential for this analysis [74–77]. The most critical of these are outlined below.

- For a compact model to be physically viable, its metric components must be non-singular, finite, and strictly positive at all points within the configuration.
- For a stellar model to be considered physically realistic, its interior energy density and pressure profiles must satisfy a set of essential criteria. Both the energy density and pressure components must remain strictly positive throughout the stellar interior. It is also necessary for every thermodynamic quantity to be finite and non-singular throughout the entire system. Furthermore, these

parameters must be centrally maximized and decrease monotonically in a smooth manner from the core to the surface. The gradients of both the energy density and radial pressure must vanish at $r = 0$ and remain strictly negative throughout the rest of the stellar interior.

- It is confirmed that there is no point mass at the origin since the mass enclosed within a radius r, described by Eq. (13), approaches zero as $r \to 0$. This function illustrates the distribution of mass inside the arrangement by showing a constant positive growth as r grows. The mass to radius ratio, which defines compactness, is a crucial notion for assessing the equilibrium state and gravitational binding of an object. Celestial objects with extreme density, such as neutron stars, exhibit pronounced gravitational effects due to their exceptionally high compactness. For a highly dense object to remain stable, Buchdahl [78] demonstrated that its compactness $\mu = \frac{m}{r}$ must not exceed the value of $\frac{4}{9}$.
- Surface redshift is a well-documented phenomenon in which light escaping a strong gravitational field, such as that of a massive celestial body, undergoes a shift toward longer wavelengths. The reason for this phenomenon is that gravity affects time. Light's energy decreases as it leaves a huge body's strong gravitational field, which results in redshift. The surface redshift, z_s, defined as follows, is observed to be strictly positive in astrophysical contexts

$$z_s = \left(1 - 2\mu\right)^{-\frac{1}{2}} - 1. \tag{32}$$

A physically acceptable model requires its value at Σ to be bounded by $z_s \leq 5.211$ [79].

- For the internal fluid distribution, the gravitational redshift is calculated using the expression $z_g = e^{-\chi/2} - 1$. This redshift, being determined entirely by the temporal metric, is expected to decrease monotonically towards the surface.
- For compact stellar objects, the radial and transverse pressures are related to the energy density by the equations of state $p_r = \omega_r \rho$ and $p_t = \omega_t \rho$, where ω_r and ω_t are the respective parameters. This relation governs fundamental characteristics like the mass-radius ratio, stability, and maximum mass limit for compact stars. The corresponding formal expression is given by

$$\omega_r = \frac{p_r}{\rho}, \quad \omega_t = \frac{p_t}{\rho}. \tag{33}$$

A fundamental criterion for physically realistic matter is that these ratios fall within the interval [0, 1]. Such solutions are thermodynamically admissible for describing stellar interiors.

- The description of physically plausible matter in stellar cores requires the interior fluid to satisfy specific energy conditions. Within this formalism, the corresponding expressions are

$$\left.\begin{aligned} &\rho + \frac{q^2}{r^4} \geq 0, \quad \rho + p_r \geq 0, \quad \rho - p_t \geq 0, \\ &\rho + p_t + \frac{2q^2}{r^4} \geq 0, \quad \rho - p_r + \frac{2q^2}{r^4} \geq 0, \\ &\rho - p_r - 2p_t \geq 0, \quad \rho + p_r + 2p_t + \frac{2q^2}{r^4} \geq 0. \end{aligned}\right\} \tag{34}$$

The most critical constraints are the dominant and trace energy conditions. These require that throughout the system, the energy density must be non-negative and must dominate over the radial pressure (accounting for electromagnetic effects), the tangential pressure, and the combined stress $p_r + 2p_t$. Formally, these are expressed as $\rho - p_r + \frac{2q^2}{r^4} \geq 0$, $\rho - p_t \geq 0$ and $\rho - p_r - 2p_t \geq 0$.

- The moment of inertia is another crucial characteristic that must be carefully considered when describing compact stars. It calculates the distribution of mass with respect to the rotational axis. A star's evolutionary trajectory and structural stability are significantly influenced by its moment of inertia. The highest sustained rotational rate and maximum stable mass of a compact star are directly determined by these factors. By accurately determining the rotational inertia of a compact star empirically, the equation of state governing ultra-dense matter can be greatly reduced. This is given by [80]

$$I = \frac{2}{5}\left(1 + \frac{M}{R}\right) M R^2. \tag{35}$$

It must be mentioned here that the anisotropic pressure arises in relativistic astrophysical objects where strong gravitational fields, very high densities, magnetic fields, phase transitions, superfluid cores, or rotation can produce a difference between radial and tangential pressure. We list the rotation as one of the possible mechanisms that appear in the literature, but it will not be implemented in our solutions. The anisotropy in our work is purely local pressure anisotropy balanced against density inhomogeneity through the vanishing complexity condition. Hence, the anisotropic fluid description used here provides a convenient mathematical framework to study local pressure anisotropy independently of the specific physical mechanism that generates it.

- Hydrostatic equilibrium in stars describes a state of balance where the inward pull of gravity is precisely counteracted by outward pressure forces. This equilibrium state

is fundamentally described by the TOV equation (11), which can be recast into the following equivalent form

$$f_g + f_h + f_a + f_e = 0, \tag{36}$$

where

$$f_g = -\frac{\chi'}{2}(\rho + p_r), \quad f_h = -\frac{dp_r}{dr},$$
$$f_a = \frac{2}{r}(p_t - p_r), \quad f_e = \frac{2qq'}{r^4}.$$

In a stellar system in equilibrium, the inward gravitational force is balanced by the combined positive contributions from hydrostatic pressure, anisotropic stress, and electromagnetic repulsion. This balance of opposing forces maintains the system's stability. Hydrostatic equilibrium is achieved when the net force acting on every point within the stellar interior, for all r, is identically zero.

- The causality condition requires that the speed of sound within a medium must not exceed the speed of light [81]. A fundamental requirement for a physically admissible compact star is that the radial and tangential sound speeds remain subluminal ($0 < v_r^2,\ v_t^2 < 1$) at all interior points. These quantities are defined by the following expressions

$$v_r^2 = \frac{dp_r}{d\rho}, \quad v_t^2 = \frac{dp_t}{d\rho}. \tag{37}$$

- Analyzing the stability of celestial systems has emerged as a central focus in modern high-energy astrophysics. Herrera [82] first proposed the concept of "cracking" in self-gravitating fluids. It occurs when the net radial force reverses its direction at specific interior points. To prevent cracking, the system must fulfill the following condition

$$0 < |v_t^2 - v_r^2| < 1. \tag{38}$$

- Developed to evaluate the stability of compact objects, the Harrison–Zeldovich–Novikov criterion determines whether a gravitationally bound system will remain in equilibrium or collapse when perturbed. It provides a method for determining whether a system in equilibrium remains stable under small perturbations or becomes unstable. This criterion states that a system in equilibrium is stable, provided the derivative of its total mass with respect to the central density is positive. Mathematically, this requires $\frac{\partial M(\rho_c)}{\partial \rho_c} > 0$ [83,84].
- In dense stellar astrophysics, the adiabatic index serves as a fundamental determinant of a star's structural integrity and stability against collapse. It quantifies how pressure responds to density changes during adiabatic processes, where no heat is exchanged with the environment. A star becomes unstable and may collapse gravitationally if its adiabatic index is less than $\frac{4}{3}$ [85,86]. A stellar configuration remains stable against gravitational collapse only if its adiabatic index exceeds the critical threshold. This parameter is defined along the principal spatial directions as

$$\Gamma_r = \frac{\rho + p_r}{p_r}\frac{dp_r}{d\rho}, \quad \Gamma_t = \frac{\rho + p_t}{p_t}\frac{dp_t}{d\rho}. \tag{39}$$

5 Exact analytical models of stellar interiors

Researchers have long stressed that obtaining solutions to Einstein's field equations is fundamental for modeling the universe's gravitational phenomena. This study, therefore, aims to develop and examine potential strategies for obtaining viable solutions to this system. A number of well-defined methodologies for solving this problem have been proposed in the existing research. Our approach derives exact solutions by simultaneously imposing the vanishing complexity criterion and specifying the form of the radial metric potential. The subsections that follow provide an individual analysis for each solution.

5.1 Stellar solution 1

The system (8)–(10) is under-determined, as it comprises only three equations for the six variables ρ, p_r, p_t, χ, λ, and q. To constrain the system's degrees of freedom, we adopt a known charge distribution model as $q = \alpha r^3$ with α being a parameter having the dimension of ℓ^{-2} [87], which reduces the number of undetermined physical parameters to five. Here, α quantifies the charge intensity within the stellar interior. This particular functional form for the interior charge has been widely adopted in the literature on charged compact objects because it guarantees that the charge vanishes at the center, the electric field is zero at the center, and the charge density remains finite and regular everywhere inside the star, avoiding any singularity at $r = 0$. We, therefore, enforce the vanishing complexity condition ($Y_{TF} = 0$) and specify a known expression for the radial metric function. This particular constraint is defined as [88]

$$e^{\lambda} = \frac{7\left(r^2x + 1\right)^2}{7 - r^4x^2 - 10r^2x}, \tag{40}$$

with the constant x possessing the dimension ℓ^{-2}. Substituting this in Eq. (31) and solving this differential equation

leads to the following form for the temporal potential

$$e^{\chi}=c_2\cos^2\left[c_1+\frac{1}{2x}\left\{\sqrt{\frac{77}{2}}\sqrt{-\alpha^2}\left(\sqrt{7-r^2x\left(r^2x+10\right)}\right.\right.\right.$$
$$\left.\left.\left.+4\sin^{-1}\left(\frac{r^2x+5}{4\sqrt{2}}\right)\right)\right\}\right], \tag{41}$$

where c_1 and c_2 are constants of integration. Consequently, the fluid triplet (8)–(10) can be rewritten using the metric potentials (40) and (41) as follows

$$\rho=\frac{8x\left(r^2x\left(r^2x+2\right)+9\right)}{7\left(r^2x+1\right)^3}-\alpha^2r^2, \tag{42}$$

$$p_r=\frac{1}{r^2x+1}\left\{\tan\left(c_1\right.\right.$$
$$\left.+\frac{\sqrt{\frac{77}{2}}\sqrt{-\alpha^2}\left(\sqrt{7-r^2x\left(r^2x+10\right)}+4\sin^{-1}\left(\frac{r^2x+5}{4\sqrt{2}}\right)\right)}{2x}\right)$$
$$\left.\times\sqrt{\frac{22}{7}}\sqrt{-\alpha^2}\sqrt{7-r^2x\left(r^2x+10\right)}\right\}$$
$$+\alpha^2r^2-\frac{8x\left(r^2x+3\right)}{7\left(r^2x+1\right)^2}, \tag{43}$$

$$p_t=\frac{1}{r^2x+1}\left\{\tan\left(c_1\right.\right.$$
$$\left.+\frac{\sqrt{\frac{77}{2}}\sqrt{-\alpha^2}\left(\sqrt{7-r^2x\left(r^2x+10\right)}+4\sin^{-1}\left(\frac{r^2x+5}{4\sqrt{2}}\right)\right)}{2x}\right)$$
$$\left.\times\sqrt{\frac{22}{7}}\sqrt{-\alpha^2}\sqrt{7-r^2x\left(r^2x+10\right)}\right\}$$
$$+\frac{9\alpha^2r^2}{2}+\frac{8x\left(r^2x-3\right)}{7\left(r^2x+1\right)^3}. \tag{44}$$

The presence of anisotropic pressure indicates that the pressure within a system is not isotropic and varies along different spatial axes. This study employs a spherical geometry, and therefore, examines the main pressures in the radial and tangential directions. For this configuration, the pressure anisotropy is given by

$$\Pi=\frac{7\alpha^2r^2}{2}+\frac{8r^2x^2\left(r^2x+5\right)}{7\left(r^2x+1\right)^3}. \tag{45}$$

In relativistic astrophysics, junction conditions are essential for describing how matter and spacetime curvature behave at boundaries. A fundamental requirement for physical consistency is the continuity of the metric tensor and extrinsic curvature across an interface, as enforced by these conditions. In boundary value problems, these conditions are essential for analyzing wave propagation and disturbances, and for understanding system behavior at interfaces. At the boundary surface $r=R(>2M)$, where M denotes the total mass, the interior spacetime metric must continuously match the external Reissner–Nordström solution. This metric thus serves under the total charge Q as

$$ds^2=\left(1-\frac{2M}{r}+\frac{Q^2}{r^2}\right)dt^2-\left(1-\frac{2M}{r}+\frac{Q^2}{r^2}\right)^{-1}dr^2$$
$$-r^2\left(d\theta^2+\sin^2\theta d\phi^2\right). \tag{46}$$

The continuity of the metric functions over the boundary $r=R$ and the continuity of the extrinsic curvature are the two main postulates. The metric functions' continuity and the radial pressure's disappearance at the boundary are both guaranteed by the following mathematical expressions

$$1-\frac{2M}{R}+\frac{Q^2}{R^2}=\frac{7-R^4x^2-10R^2x}{7\left(R^2x+1\right)^2},$$
$$p_r=0=\frac{1}{R^2x+1}\left\{\sqrt{\frac{22}{7}}\sqrt{-\alpha^2}\sqrt{7-R^2x\left(R^2x+10\right)}\tan\left(c_1\right.\right.$$
$$\left.\left.+\frac{\sqrt{\frac{77}{2}}\sqrt{-\alpha^2}\left(\sqrt{7-R^2x(R^2x+10)}+4\sin^{-1}\left(\frac{R^2x+5}{4\sqrt{2}}\right)\right)}{2x}\right)\right\}$$
$$+\alpha^2R^2-\frac{8x(R^2x+3)}{7(R^2x+1)^2}. \tag{47}$$

By simultaneously solving the system, the constants (x, c_1) are found, yielding the following expressions

$$x=\frac{4\sqrt{R^6\left(-14MR+7Q^2+9R^2\right)}+2R^3(7M-6R)-7Q^2R^2}{R^4\left(2R(4R-7M)+7Q^2\right)},$$
$$c_1=\frac{1}{4x\sqrt{-\alpha^2}}\left[4\pi\sqrt{-\alpha^2}c_1x\right.$$
$$+\sqrt{154}\alpha^2\left\{\sqrt{7-R^2x(R^2x+10)}-4\alpha x\right.$$
$$\times\tanh^{-1}\left(\frac{7\alpha^2R^2(R^2x+1)^2-8x(R^2x+3)}{\sqrt{154}\sqrt{7-R^2x(R^2x+10)}(\alpha+\alpha R^2x)}\right)$$
$$\left.\left.+4\sin^{-1}\left(\frac{R^2x+5}{4\sqrt{2}}\right)\right\}\right]. \tag{48}$$

The Harrison–Zeldovich–Novikov static stability condition and the mass function for this model are

$$m=\frac{1}{70}r\left\{\frac{40r^2x\left(r^2x+3\right)}{\left(r^2x+1\right)^2}-7\alpha^2r^4\right\}, \tag{49}$$

Table 1 Estimated data of different stars [89–92]

Stars	Mass ($M_\odot$)	Radius (km)
PSR J1614 − 2230 (S1)	1.97 ± 0.04	9.69 ± 0.2
PSR J1903 + 327 (S2)	1.667 ± 0.021	9.48 ± 0.03
4U 1608 − 52 (S3)	1.74 ± 0.01	9.3 ± 0.10
Vela X − 1 (S4)	1.77 ± 0.08	9.560 ± 0.08
4U 1820 − 30 (S5)	1.58 ± 0.06	9.1 ± 0.4
Cen X − 3 (S6)	1.49 ± 0.08	9.178 ± 0.13
SMC X − 4 (S7)	1.29 ± 0.05	8.831 ± 0.09
LMC X − 4 (S8)	1.04 ± 0.09	8.301 ± 0.2

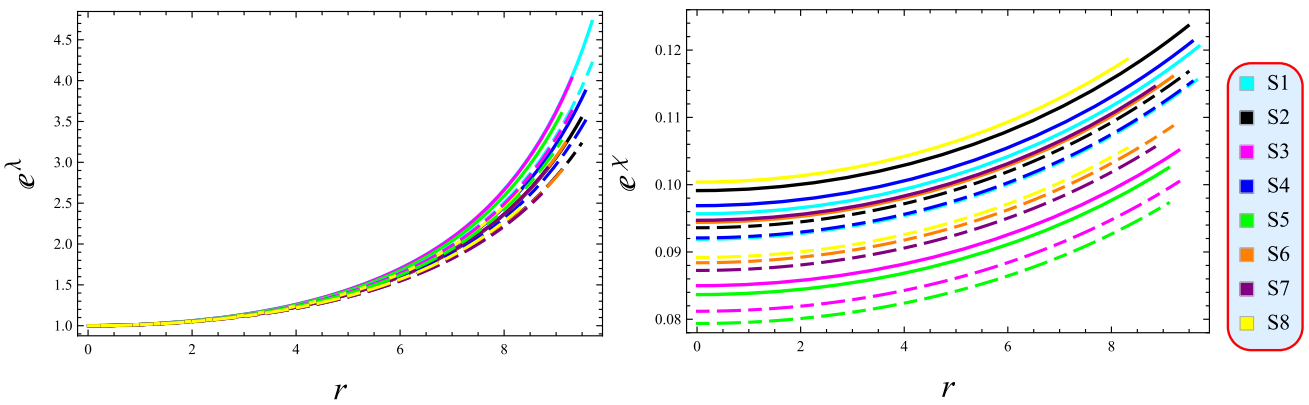

Fig. 1 Metric components for solution 1 at $Q = 2$ (thick) and 2.2 (dashed)

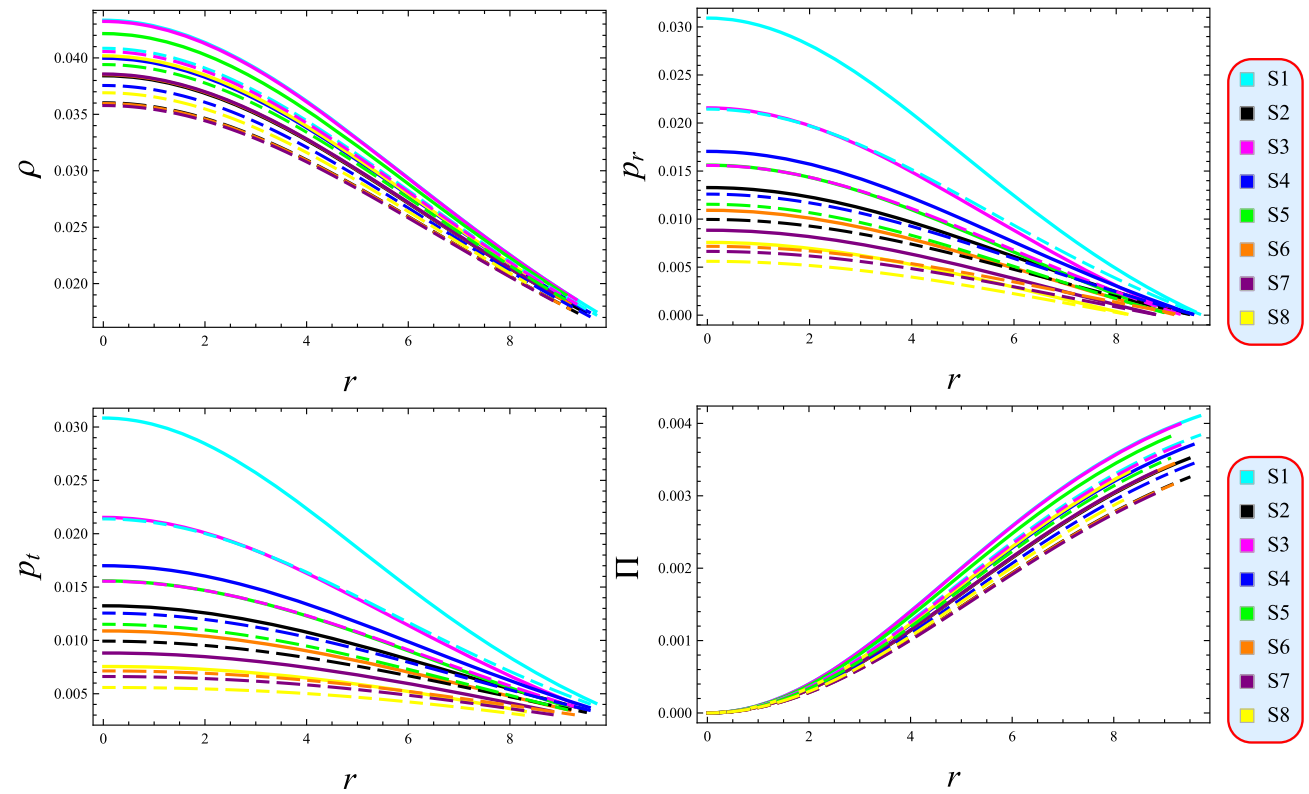

Fig. 2 Governing variables for solution 1 at $Q = 2$ (thick) and 2.2 (dashed)

$$M(\rho_c) = \frac{1}{70} R \left\{ \frac{280 R^2 \rho_c \left(7R^2\rho_c + 216\right)}{\left(7R^2\rho_c + 72\right)^2} - 7\alpha^2 R^4 \right\}. \tag{50}$$

The developed solution undergoes a thorough physical investigation with an emphasis on its stability behavior and internal characteristics. Basic properties of the solution's stability are revealed by analyzing it under various physical circumstances as well as external stimuli. We assume the estimated masses and radii of five compact stars in order to assess the impact of electric charge in Table 1 by taking into account charge parameter values of $Q = 2, 2.2$. Notably, the values of the total charge Q are not chosen arbitrarily but are those required for the vanishing-complexity models to correctly describe the observed mass-radius data of the selected pulsars. These Q values lie in the range that keeps the configurations far from the extremal Reissner–Nordström limit ($Q < M$ in geometric units), and are consistent with the charge magnitudes typically considered in the recent literature on charged compact objects. On the other hand, one can consider the values of Q from the relation $\alpha = Q/R^3$ which holds at the boundary. Since fundamental physical charac-

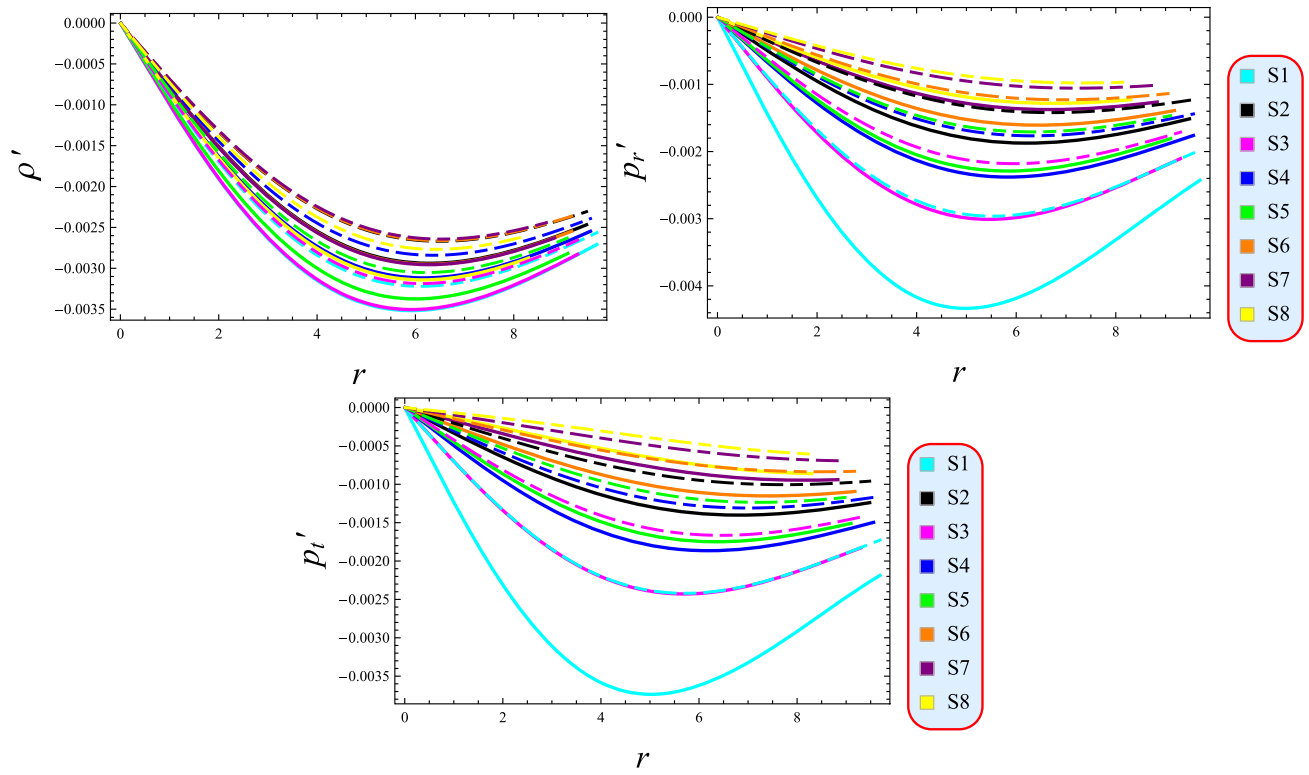

Fig. 3 Regularity conditions for solution 1 at $Q = 2$ (thick) and 2.2 (dashed)

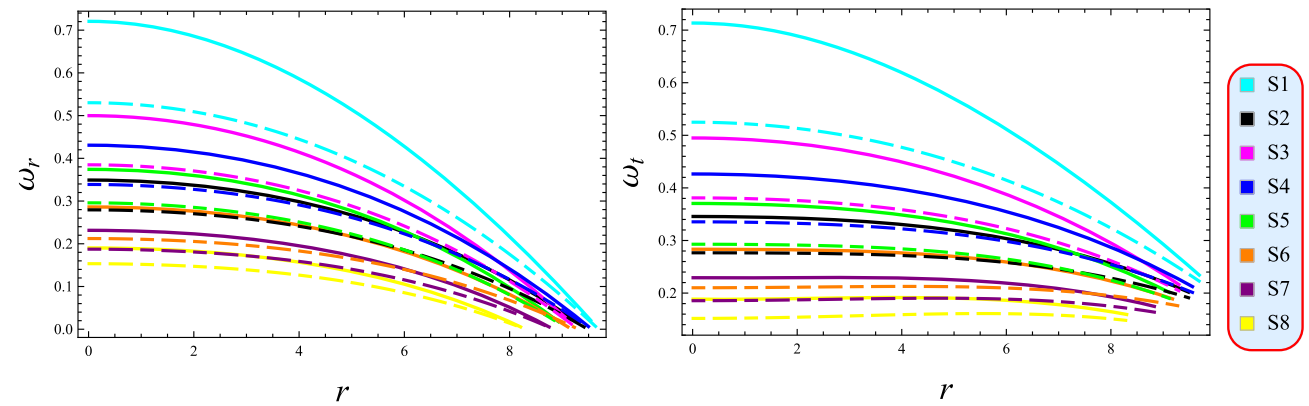

Fig. 4 Realistic parameters for solution 1 at $Q = 2$ (thick) and 2.2 (dashed)

teristics dictate whether the solutions are feasible in realistic situations, our study starts by looking into how the matter variables and metric coefficients behave. The metric potentials, which are bounded between (0, 1], are the first thing we examine. The radial potential achieves unity at the star's center, after which both metric components grow monotonically in the direction of the outer boundary. For both values, the profiles shown in Fig. 1 exhibit smooth and physically permissible behavior, remaining positive-definite throughout the stellar interior.

The evolution of the matter variables and anisotropy is depicted in Fig. 2. At the star core, the tangential pressure, radial pressure, and energy density all reach their maximum values. The star's energy density decreases monotonically from the core to the surface, staying positive and finite throughout. The radial pressure remains positive throughout the star as it steadily decreases from its greatest at the core to zero at the surface. From the core to the surface, the tangential pressure remains decreasing. The pressure rises from the core, peaks in the center of the star, and then declines steadily in the direction of the stellar surface. Fundamental physical

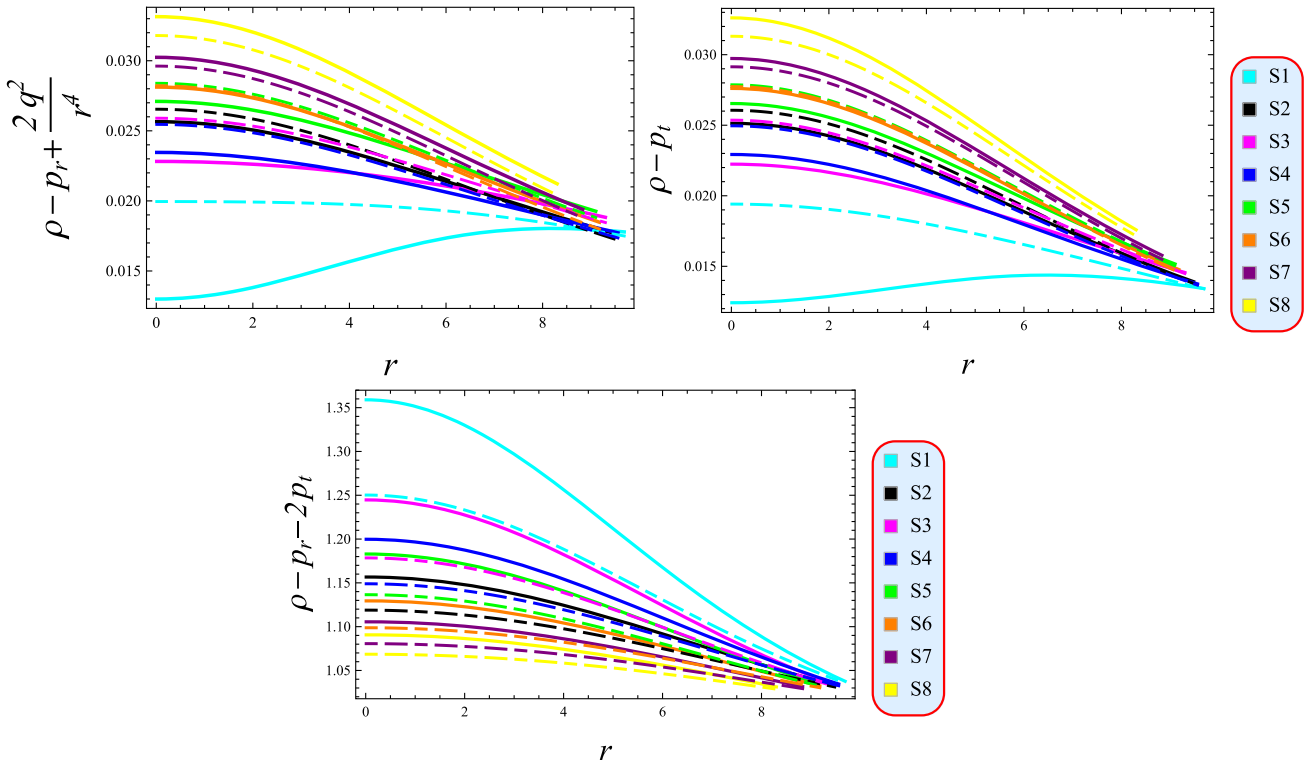

Fig. 5 Viability for solution 1 at $Q = 2$ (thick) and 2.2 (dashed)

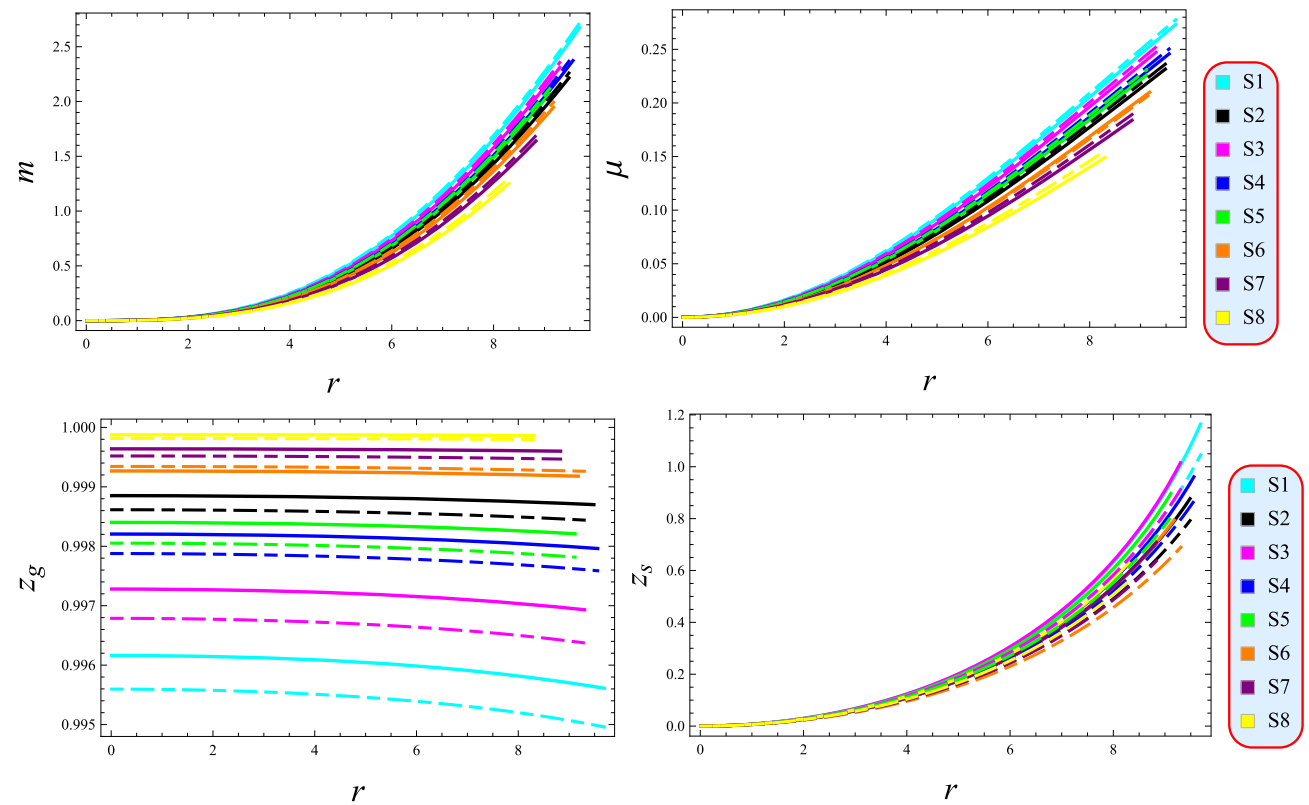

Fig. 6 Mass dependent factors for solution 1 at $Q = 2$ (thick) and 2.2 (dashed)

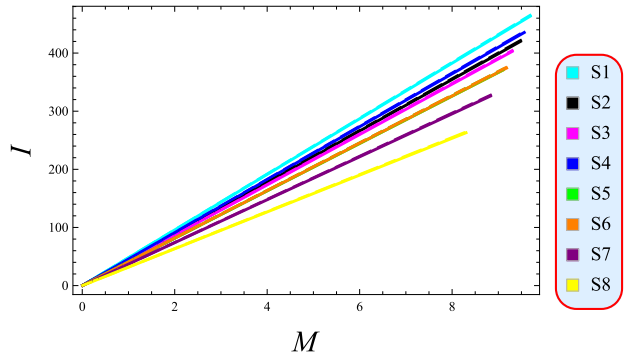

Fig. 7 Moment of inertia for solution 1 at $Q = 2$ (thick) and 2.2 (dashed)

restrictions are satisfied since the tangential pressure gradually decreases to preserve finite values at the surface. There is zero anisotropy at the core since the tangential and radial pressures are equal. The rate of change of physical quantities in relation to the radial coordinate inside the star is described by the radial gradient. Gradients quantify the radial variation of fluid properties within the star and can be used to evaluate the physical validity of the solution. Both the radial pressure and energy density must have negative second derivatives and zero first derivatives at the center ($r = 0$) for a regular solution. The models successfully satisfy these requirements and exhibit the anticipated physical consistency, as shown in Fig. 3.

For a realistic star model, the energy density to pressure ratios specified in Eq. (33) have to adhere to accepted physical constraints. Meeting these requirements demonstrates that the model complies with the basic thermodynamic principles governing star matter. Both parameters in Fig. 4 maintain values less than one over the whole star configuration, confirming that the model is density-dominated. From the center to the surface, fluid characteristics like density and pressure decrease monotonically. In order to verify the physical validity of the solution, we further examine the energy conditions across the star interior. The research confirms that this solution is physically consistent as Fig. 5 shows that the fluid properties in the star's core behave properly. The mass function's radially growing profile, which approaches zero at $r = 0$, is depicted in Fig. 6. The compactness of an object, defined by its mass relative to its radius is a key factor governing its gravitational binding energy and structural integrity. This work show that configuration are only physically admissible if they adhere to the compactness limit $\mu < 0.44$. Furthermore, it is shown that the surface redshift remains within its permissible theoretical range, verifying the solution's physical admissibility. As shown in Fig. 7, the moment of inertia increases monotonically with stellar mass, confirming a positive correlation. Figure 8 shows the force distribution within the solution, confirming the establishment of hydrostatic balance. Figure 9 verifies that the solution meets all four stability criteria, confirming its dynamical stability.

5.2 Stellar solution 2

The physical properties of an alternative stellar solution, constructed from a particular ansatz for the radial metric, are investigated in this subsection. This is defined according as [93]

$$e^{\lambda} = \frac{1}{r^4 x - r^2 y + 1}, \tag{51}$$

where x and y are constants, both carrying dimensions of ℓ^{-4} and ℓ^{-2}. Solving the differential equation derived from substituting this into Eq. (31), we get

$$e^{\chi} = c_4 \cos^2\left(\frac{\sqrt{22}\sqrt{-\alpha^2}\ln\left(2r^2x + 2\sqrt{x}\sqrt{r^4x - r^2y + 1} - y\right)}{4\sqrt{x}} - c_3\right), \tag{52}$$

where c_3 and c_4 represent constants of integration. Applying Eqs. (51) and (52) to the fluid triplet (8)–(10) yields

$$\rho = 3y - r^2\left(\alpha^2 + 5x\right), \tag{53}$$

$$p_r = -\tan\left(\frac{\sqrt{22}\sqrt{-\alpha^2}\ln(2r^2x + 2\sqrt{x}\sqrt{r^4x - r^2y + 1} - y)}{4\sqrt{x}} - c_3\right) \times \sqrt{22}\sqrt{-\alpha^2}\sqrt{r^4x - r^2y + 1} + r^2(\alpha^2 + x) - y, \tag{54}$$

$$p_t = -\tan\left(\frac{\sqrt{22}\sqrt{-\alpha^2}\ln(2r^2x + 2\sqrt{x}\sqrt{r^4x - r^2y + 1} - y)}{4\sqrt{x}} - c_3\right) \times \sqrt{22}\sqrt{-\alpha^2}\sqrt{r^4x - r^2y + 1} + r^2(9\alpha^2/2 + 2x) - y, \tag{55}$$

where the resulting pressure anisotropy is

$$\Pi = \frac{1}{2}r^2\left(7\alpha^2 + 2x\right). \tag{56}$$

To satisfy the Darmois matching conditions, the exterior spacetime of a spherical star must be static and spherically symmetric, with metric components depending exclusively on the radial coordinate r. The Reissner–Nordström metric, previously defined in Eq. (46), is used to apply the matching conditions, yielding

$$1 - \frac{2M}{R} + \frac{Q^2}{R^2} = R^4x - R^2y + 1, \tag{57}$$

$$p_r = 0 = R^2(\alpha^2 + x) - y - \sqrt{22}\sqrt{-\alpha^2}\sqrt{R^4x - R^2y + 1} \times \tan\left(\frac{\sqrt{22}\sqrt{-\alpha^2}\ln\left(2R^2x + 2\sqrt{x}\sqrt{R^4x - R^2y + 1} - y\right)}{4\sqrt{x}} - c_3\right).$$

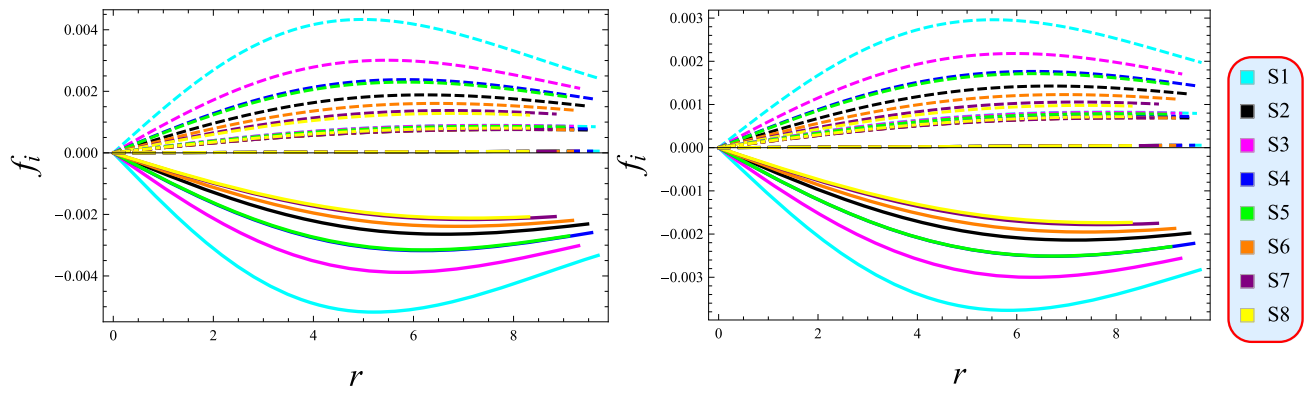

Fig. 8 Balance of forces for solution 1 corresponding to f_g (thick), f_h (dashed) and f_a (dot-dashed) at $Q = 2$ (left) and 2.2 (right)

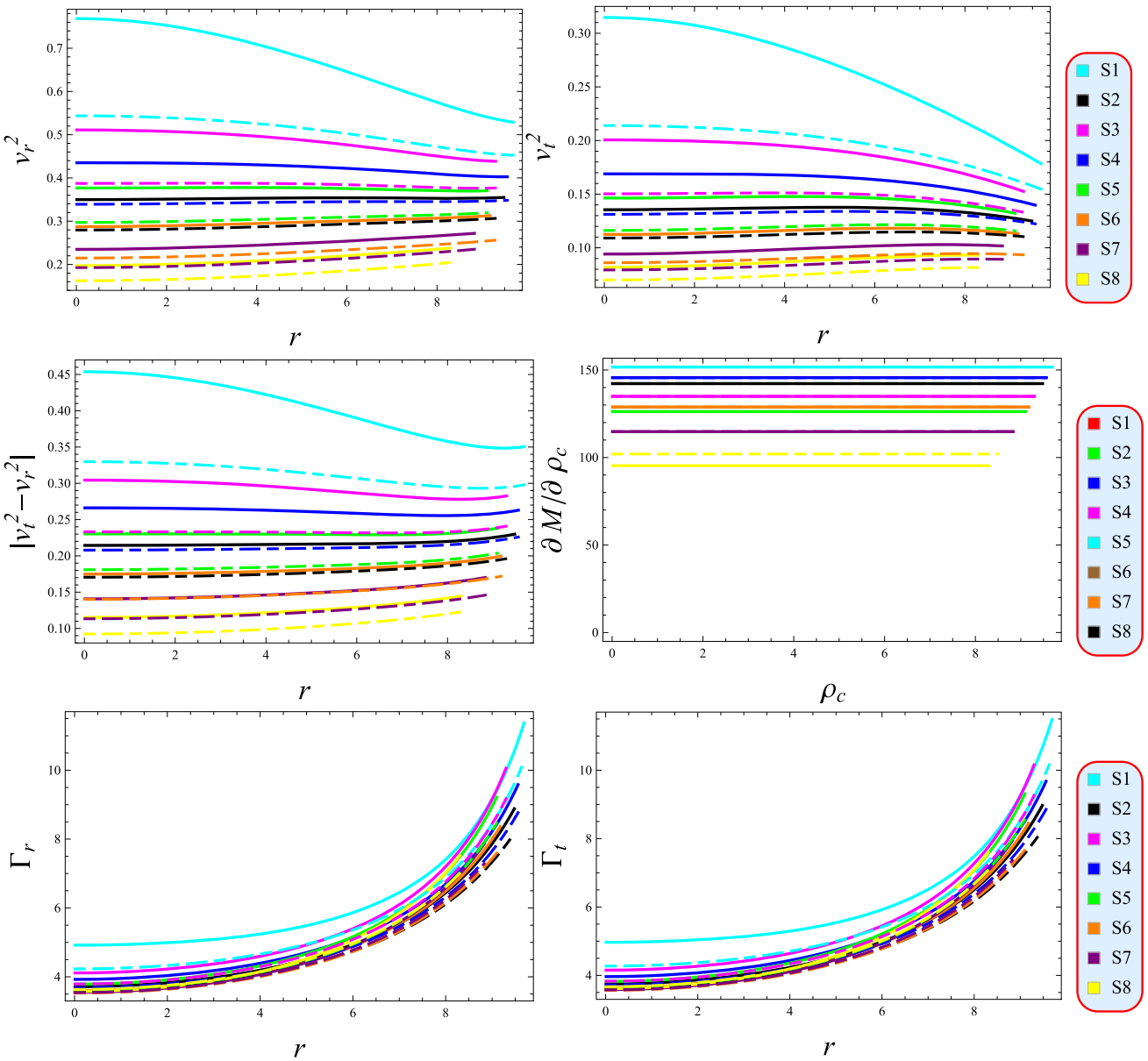

Fig. 9 Stability analysis for solution 1 at $Q = 2$ (thick) and 2.2 (dashed)

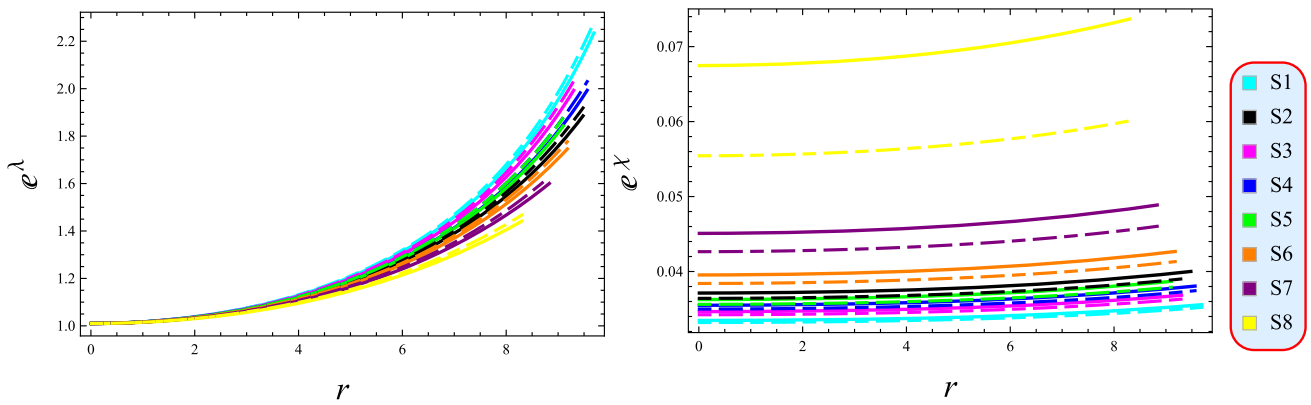

Fig. 10 Metric components for solution 2 at $Q = 2$ (thick) and 2.2 (dashed)

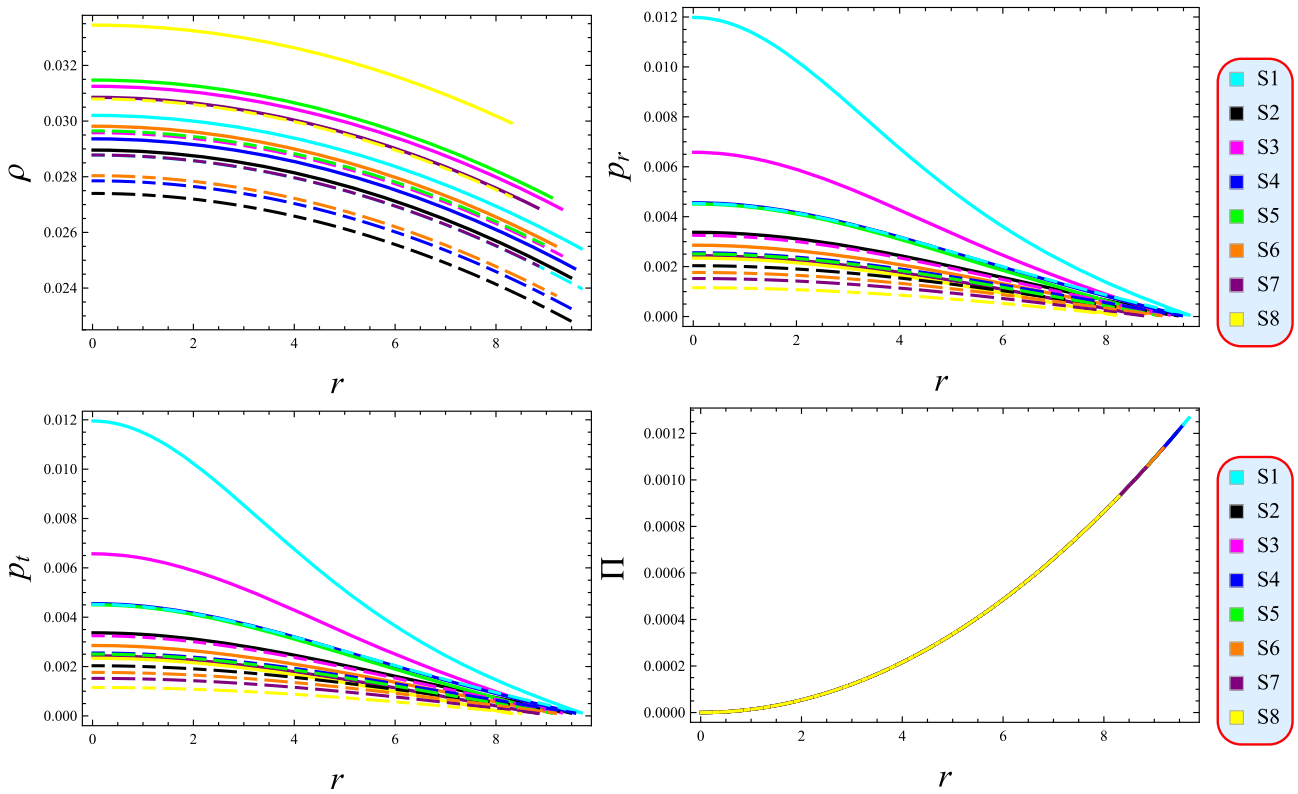

Fig. 11 Governing variables for solution 2 at $Q = 2$ (thick) and 2.2 (dashed)

We solve this system simultaneously to obtain the constants (y, c_3) as

$$y = \frac{2MR - Q^2 + R^6 x}{R^4}, \tag{58}$$

$$c_3 = \pi c_5 + \frac{\sqrt{\frac{11}{2}}\sqrt{-\alpha^2}\ln\left(2R^2x + 2\sqrt{x}\sqrt{R^4x - R^2y + 1} - y\right)}{2\sqrt{x}} + \tan^{-1}\left(\frac{y - R^2(\alpha^2 + x)}{\sqrt{22}\sqrt{-\alpha^2}\sqrt{R^4x - R^2y + 1}}\right), \tag{59}$$

with c_5 being an integer. Furthermore, the model defines both the mass function and the Harrison–Zeldovich–Novikov stability condition as follows

$$m = \frac{1}{10}\left\{5r^3y - r^5\left(\alpha^2 + 5x\right)\right\}, \tag{60}$$

$$M(\rho_c) = \frac{1}{30}\left\{5R^3\rho_c - 3R^5\left(\alpha^2 + 5x\right)\right\}. \tag{61}$$

We now evaluate the derived solution against the observational data in Table 1. An analysis of the metric potentials

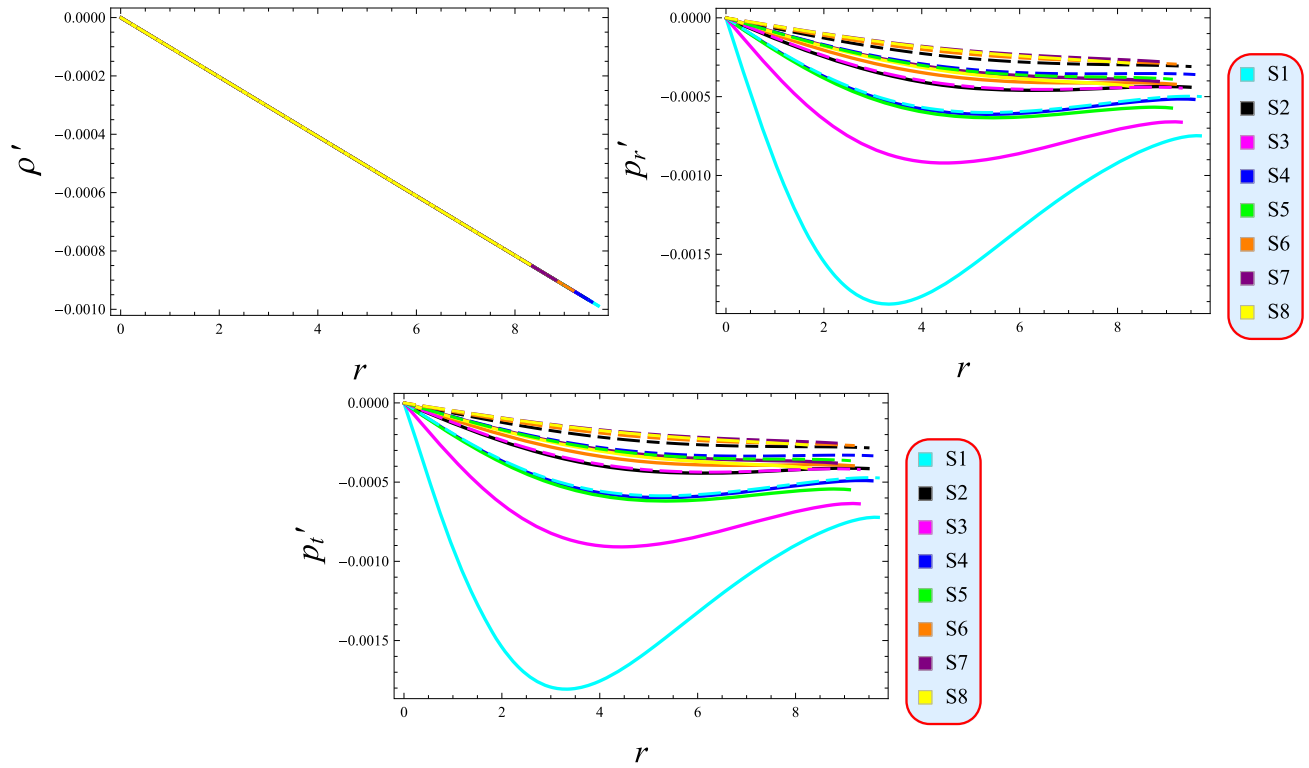

Fig. 12 Regularity conditions for solution 2 at $Q = 2$ (thick) and 2.2 (dashed)

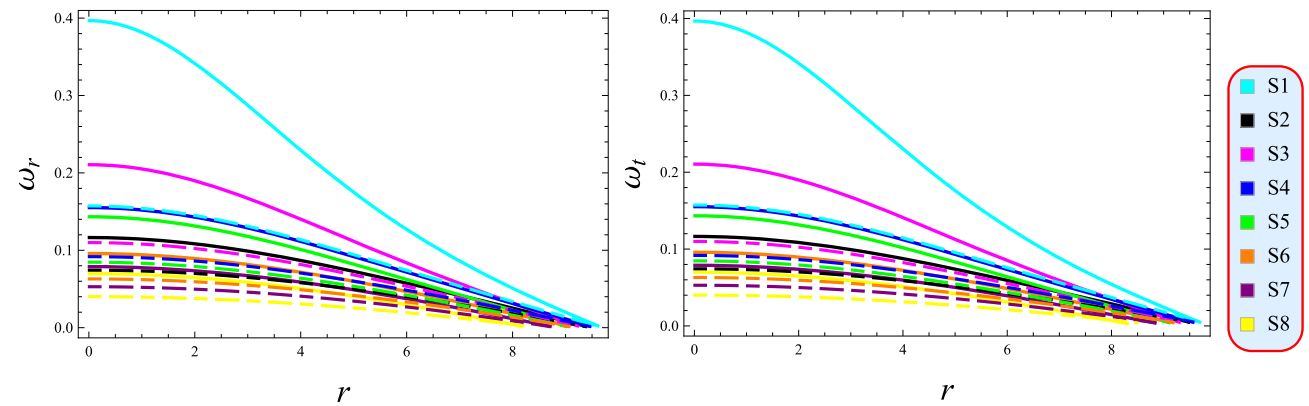

Fig. 13 Realistic parameters for solution 2 at $Q = 2$ (thick) and 2.2 (dashed)

confirms that this model exhibits regularity and behavior consistent with the previous solution. As shown in Fig. 10, the metric components exhibit smooth, positive, and monotonically increasing behavior across the entire domain. Figure 11 shows the behavior of the matter variables, which adhere to the required physical constraints. The regularity conditions are further evaluated by analyzing radial gradients, which characterize the spatial variation of physical parameters. Analyzing the behavior of these gradient serves as a key indicator for assessing the model's physical validity. Figure 12 confirms the physical acceptability of the parameters through their well-behaved profile. All fluid variables decrease monotonically towards the stellar surface, as illustrated by the radially decreasing profiles of the parameters in Fig. 13. For a compact stellar object to be physically viable, certain regularity requirements must be fulfilled. A physically normal fluid configuration is shown in Fig. 14, which also verifies that the system complies with all necessary bounds.

The validity of the stellar model's demonstrated by the physically realistic mass, compactness, and surface redshift as depicted in Fig. 15. This model supports a higher max-

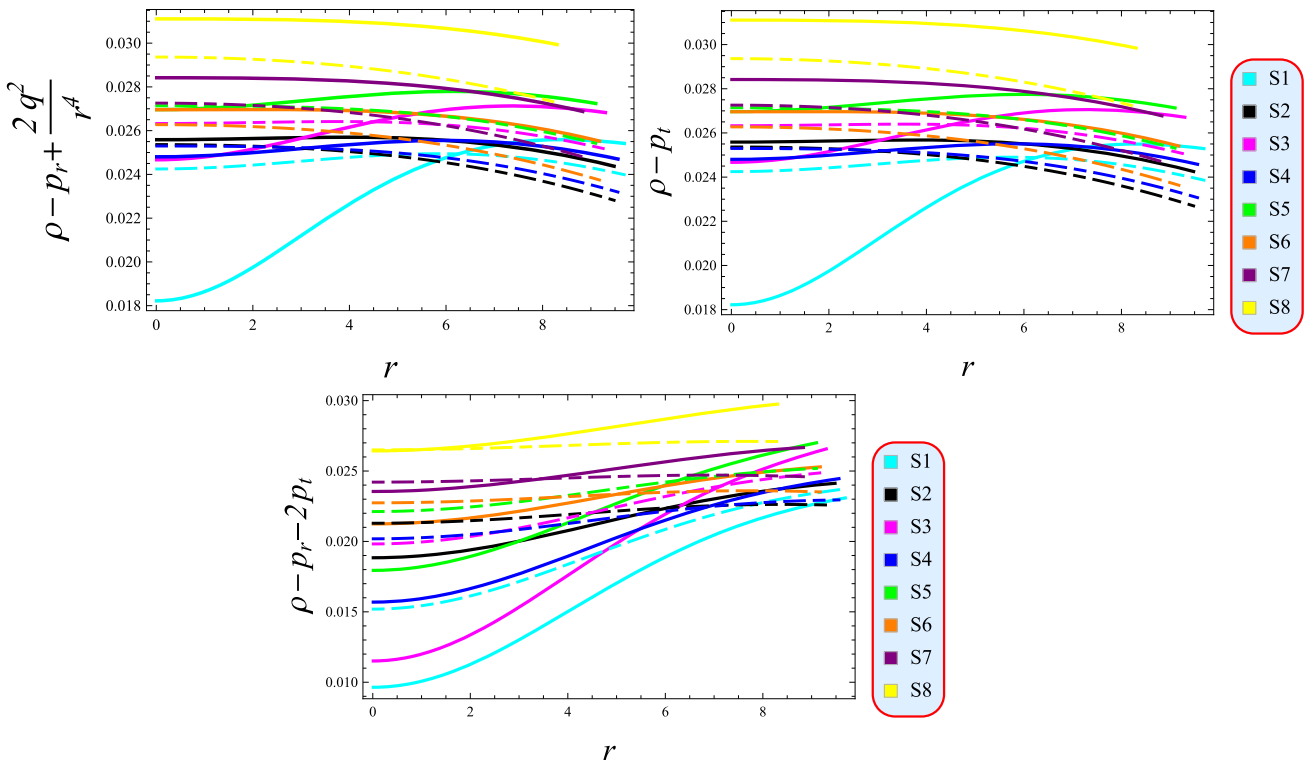

Fig. 14 Viability for solution 2 at $Q = 2$ (thick) and 2.2 (dashed)

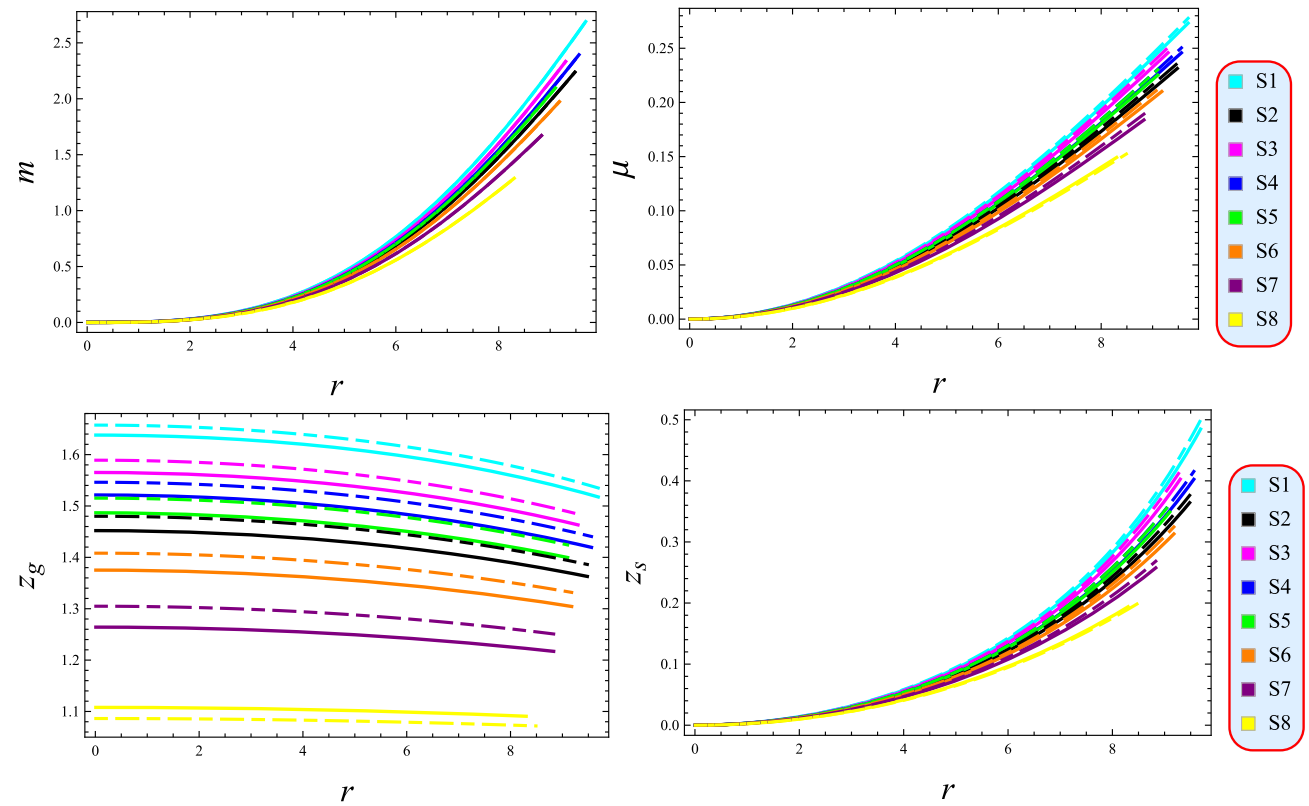

Fig. 15 Mass dependent factors for solution 2 at $Q = 2$ (thick) and 2.2 (dashed)

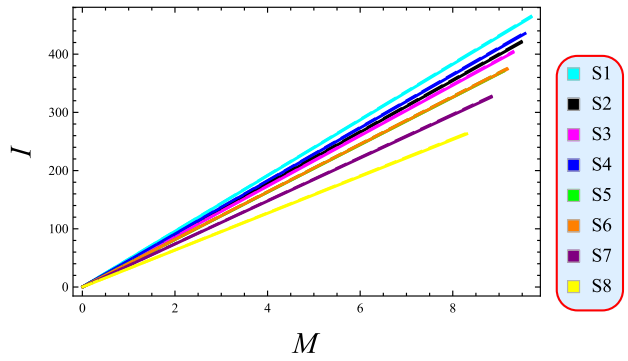

Fig. 16 Moment of inertia for solution 2 at $Q = 2$ (thick) and 2.2 (dashed)

imum mass than the previous solution, according to our investigation. The rotational dynamics of the star is directly governed by its mass distribution, which is quantified by its moment of inertia. In Fig. 16, the radial profile is constant over the whole stellar structure. We examine the model's equilibrium point, or the situation in which all opposing forces are in balance, in order to assess its stability. The system is confirmed to be in equilibrium when the vector sum of all applied forces is zero, as shown in Fig. 17. Figure 18 demonstrates the model's dynamical stability and its compliance with all four necessary physical requirements.

6 Summary, conclusions and future directions

We have derived and examined two distinct, physically permissible solutions to the Einstein–Maxwell field equations in this work. Our methodology involves solving the gravitational field equations coupled with the TOV equation for a static, spherically symmetric source. We have also derived the mass function through both geometric and energy density formulations. Via the orthogonal decomposition of the curvature tensor, we have constructed four scalars that elucidate specific physical characteristics of the system. In accordance with Herrera's framework [48], the quantity Y_{TF} has been adopted as the complexity factor for our system, as it comprehensively encodes the effects of energy density inhomogeneity and pressure anisotropy. Since the field equations (8)–(10) form an under-determined system with six unknowns (three for matter, one for charge, and two for the metric), we introduced specific constraints to derive a physically admissible solution. The requirement for a system with no complexity, as defined by Herrera's framework, is given by Eq. (30). This yielded two separate solutions, each derived by specifying a distinct form for the radial metric potential while maintaining the same predefined charge distribution. By ensuring a smooth correspondence between the interior and exterior geometries, the junction conditions at the stellar surface determined the integration constants. A set of physical requirements for realistic stellar models has been developed in this study. The main findings are summarized below.

- It is confirmed that both metric potentials are physically admissible since they are finite at the origin, increase monotonically, and remain regular throughout the star. Each component's behavior is depicted in Figs. 1 and 10. The behavior of the matter variables, detailed in Figs. 2 and 11, satisfying all necessary requirements, confirming their physical feasibility for modeling compact stars. A repulsive force is produced by the pressure anisotropy, which decreases in the core and increases towards the surface. Preventing gravitational collapse and maintaining hydrostatic equilibrium both depends on this repulsive force. Both solutions' physical validity is confirmed by the well-behaved radial gradients in Figs. 3 and 12.
- The equations of state of each matter distribution determine its distinct physical features, and Figs. 4 and 13 show this relationship. Figures 5 and 14 confirm that both solutions adhere to all energy conditions, indicating their physical plausibility.
- A stable stellar model requires that the mass and compactness profiles exhibit peak at the surface and monotonically decreasing towards the center. The redshift increases monotonically from the center to its maximum value at the stellar surface, as seen in Figs. 6 and 15. The relation between the moment of inertia and total mass is shown to be directly correlated in Figs. 7 and 16.
- Figures 8 and 17 demonstrate a diminishing net force throughout the star interior, indicating that both models maintain hydrostatic equilibrium. Both radial and transverse sound speeds continuously remain within the necessary bound, indicating that both models exhibit stability under cracking and sound speed examinations. Figures 9 and 18 demonstrate that both solutions have adiabatic indices that are compatible with stability and meet Zeldovich's requirement.

The zero complexity framework simplifies a very complex system by effectively generating physically realistic star models by combining both pressure anisotropy and density gradients. This method improved our knowledge of equilibrium in self-gravitating systems exposed to electromagnetic fields by producing stable anisotropic charged structures. The formalism provides a more profound view into stellar evolution under Einstein gravity by efficiently reducing complexity without compromising its physical integrity. This paradigm should be extended to modified gravity in future research, providing new opportunities to comprehend structural formation in a wider variety of astrophysical phenomena. This approach could be used in future research to better model compact objects and their role in the universe

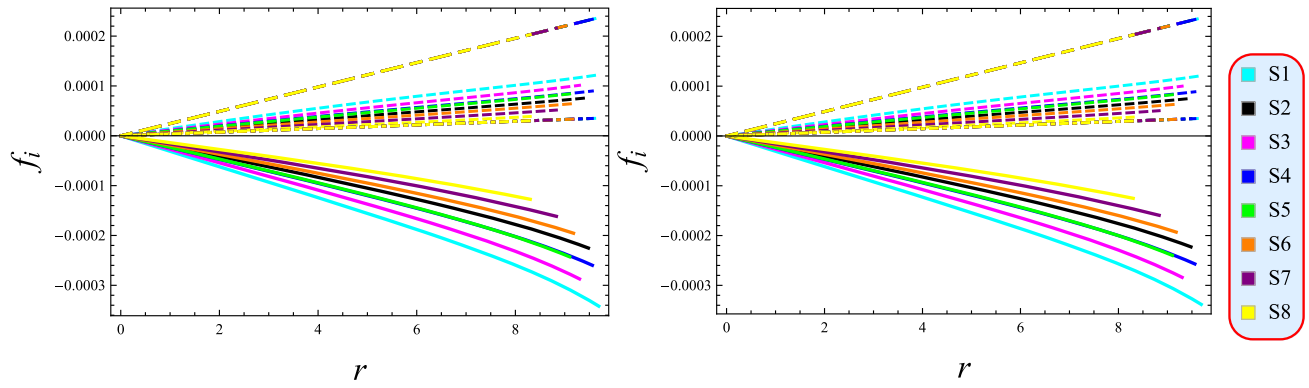

Fig. 17 Balance of forces for solution 2 corresponding to f_g (thick), f_h (dashed) and f_a (dot-dashed) at $Q = 2$ (left) and 2.2 (right)

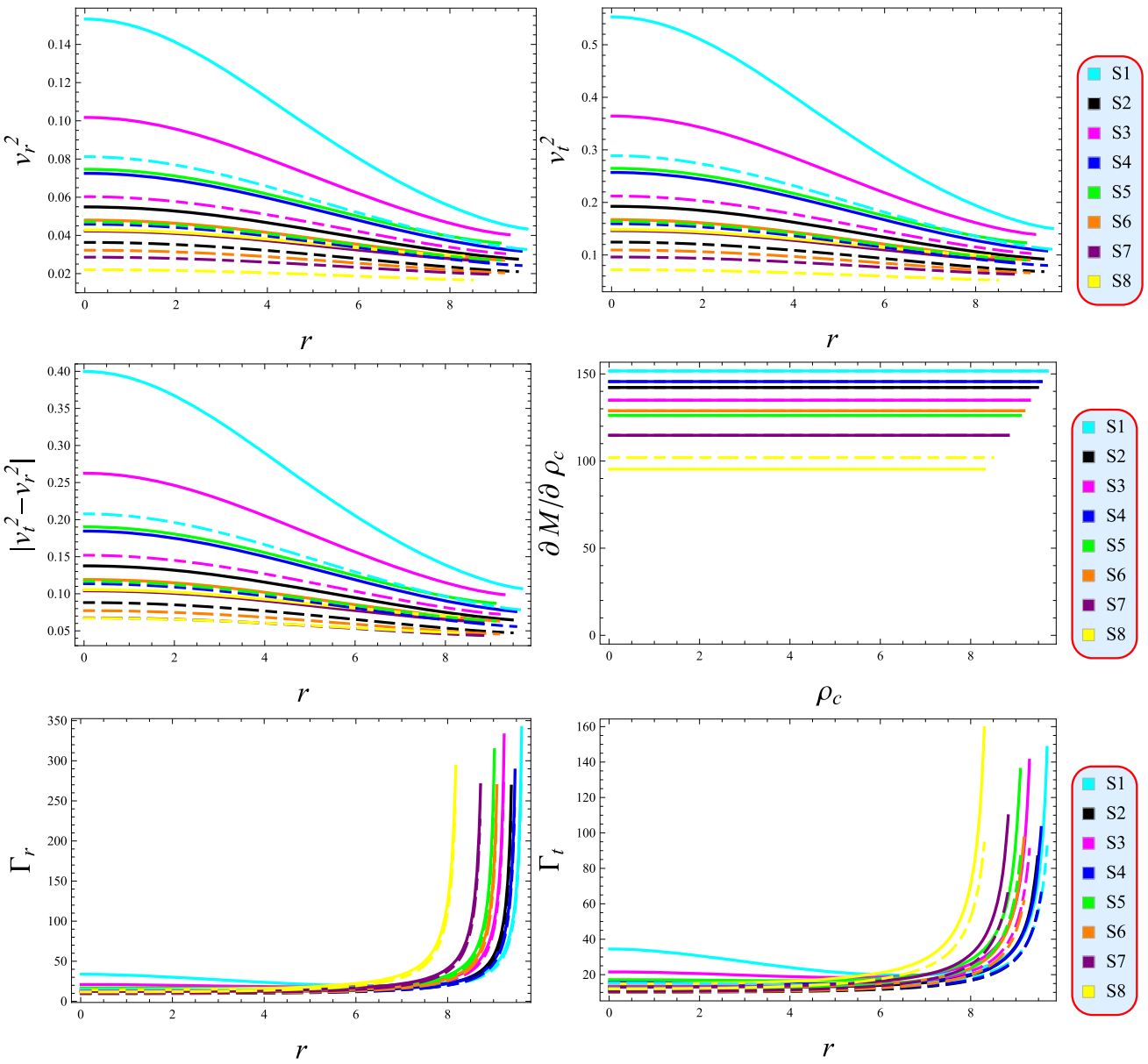

Fig. 18 Stability analysis for solution 2 at $Q = 2$ (thick) and 2.2 (dashed)

by applying gravitational wave observations as constraints to dynamic stellar evolution.

Acknowledgements The authors extend their appreciation to the Deanship of Research and Graduate Studies at King Khalid University for funding this work through Large Research Project under grant number RGP2/678/46.

Data Availability Statement No data was used for the research described in this paper. [Authors' comment: Data sharing not applicable to this article as no datasets were generated or analysed during the current study.]

Code Availability Statement This manuscript has no associated code/software. [Authors' comment: Code/Software sharing not applicable to this article as no code/software was generated or analysed during the current study.]

Funded by SCOAP[3].

References

1. L. Herrera, N.O. Santos, Phys. Rep. **286**, 53 (1997)
2. J. Ovalle, Phys. Rev. D **95**, 104019 (2017)
3. J. Ovalle, R. Casadio, R. da Rocha, A. Sotomayor, Eur. Phys. J. C **78**, 122 (2018)
4. L. Herrera, Phys. Rev. D **101**, 104024 (2020)
5. L. Herrera, J. Ospino, A. Di Prisco, Phys. Rev. D **77**, 027502 (2008)
6. G. Abellán, P. Bargueño, E. Contreras, E. Fuenmayor, Int. J. Mod. Phys. D **29**, 2050082 (2020)
7. S. Chandrasekhar, Mon. Not. R. Astron. Soc. **93**, 390 (1933)
8. F.K. Liu, Mon. Not. R. Astron. Soc. **281**, 1197 (1996)
9. G. Abellán, E. Fuenmayor, L. Herrera, Phys. Dark Universe **28**, 100549 (2020)
10. R.F. Tooper, Astrophys. J. **140**, 434 (1964)
11. S.A. Bludman, Astrophys. J. **183**, 637 (1973)
12. L. Herrera, W. Barreto, Phys. Rev. D **88**, 084022 (2013)
13. L. Herrera, A. Di Prisco, W. Barreto, J. Ospino, Gen. Relativ. Gravit. **46**, 1827 (2014)
14. G. Abellán, E. Fuenmayor, E. Contreras, L. Herrera, Phys. Dark Universe **30**, 100632 (2020)
15. K.R. Karmarkar, Proc. Indian Acad. Sci.-Sect. A **27**, 56 (1948)
16. K.N. Singh, S.K. Maurya, F. Rahaman, F. Tello-Ortiz, Eur. Phys. J. C **79**, 381 (2019)
17. J. Ospino, L.A. Núñez, Eur. Phys. J. C **80**, 166 (2020)
18. A. Ramos, C. Arias, E. Fuenmayor, E. Contreras, Eur. Phys. J. C **81**, 203 (2021)
19. M. Sharif, T. Naseer, Phys. Scr. **97**, 055004 (2022)
20. L. Herrera, A. Di Prisco, J. Ospino, E. Fuenmayor, J. Math. Phys. **42**, 2129 (2001)
21. J. Jeans, Mon. Not. R. Astron. Soc. **82**, 122 (1922)
22. M. Ruderman, Annu. Rev. Astron. Astrophys. **10**, 427 (1972)
23. V. Canuto, Annu. Rev. Astron. Astrophys. **12**, 167 (1974)
24. S.S. Yazadjiev, Phys. Rev. D **85**, 044030 (2012)
25. C.Y. Cardall, M. Prakash, J.M. Lattimer, Astrophys. J. **554**, 322 (2001)
26. V. Ioka, M. Sasaki, Astrophys. J. **600**, 296 (2004)
27. R. Ciolfi, V. Ferrari, L. Gualtieri, Mon. Not. R. Astron. Soc. **406**, 2540 (2010)
28. R.F. Sawyer, Phys. Rev. Lett. **29**, 382 (1972)
29. H. Heiselberg, M. Hjorth-Jensen, Phys. Rep. **328**, 237 (2000)
30. R.L. Bowers, E.P.T. Liang, Astrophys. J. **188**, 657 (1974)
31. M. Sharif, T. Naseer, Eur. Phys. J. Plus **139**, 296 (2024)
32. R. Sharma, S. Das, M. Govender, D.M. Pandya, Ann. Phys. **414**, 168079 (2020)
33. R.S. Bogadi, M. Govender, S. Moyo, Eur. Phys. J. C **81**, 922 (2021)
34. S. Das, B.K. Parida, R. Sharma, Eur. Phys. J. C **82**, 136 (2022)
35. M. Govender, W. Govender, G. Govender, K. Duffy, Eur. Phys. J. C **82**, 832 (2022)
36. R.S. Bogadi, M. Govender, S. Moyo, Eur. Phys. J. C **82**, 747 (2022)
37. S. Hansraj, M. Govender, L. Moodly, K.N. Singh, Phys. Rev. D **105**, 044030 (2022)
38. B.K. Parida, S. Das, M. Govender, Int. J. Mod. Phys. D **32**, 2350038 (2023)
39. S. Ray, S. Das, K.K. Ghosh, B.K. Parida, S.K. Pal, M. Indra, New Astron. **104**, 102069 (2023)
40. R.S. Bogadi, M. Govender, S. Moyo, Eur. Phys. J. Plus **138**, 426 (2023)
41. M. Govender, S. Das, Eur. Phys. J. C **84**, 367 (2024)
42. R.S. Bogadi, M. Govender, Chin. J. Phys. **91**, 382–391 (2024)
43. P. Bhar, K.N. Singh, S.K. Maurya, M. Govender, Phys. Dark Universe **43**, 101391 (2024)
44. S. Das, B.C. Paul, I.S. Sardar, S.K. Pal, Eur. Phys. J. C **85**, 275 (2025)
45. R. López-Ruiz, H.L. Mancini, X. Calbet, Phys. Lett. A **209**, 321 (1995)
46. X. Calbet, R. López-Ruiz, Phys. Rev. E **63**, 066116 (2001)
47. C.P. Panos, N.S. Nikolaidis, K.C. Chatzisavvas, C.C. Tsouros, Phys. Lett. A **373**, 2343 (2009)
48. L. Herrera, Phys. Rev. D **97**, 044010 (2018)
49. L. Bel, Ann. Inst. Henri Poincaré **17**, 37 (1961)
50. L. Herrera, J. Ospino, A. Di Prisco, E. Fuenmayor, O. Troconis, Phys. Rev. D **79**, 064025 (2009)
51. L. Herrera, A. Di Prisco, J. Ospino, Phys. Rev. D **98**, 104059 (2018)
52. L. Herrera, A. Di Prisco, J. Ospino, Phys. Rev. D **99**, 044049 (2019)
53. M. Sharif, I.I. Butt, Eur. Phys. J. C **78**, 688 (2018)
54. C. Arias, E. Contreras, E. Fuenmayor, A. Ramos, Ann. Phys. **436**, 168671 (2022)
55. S.K. Maurya, M. Govender, G. Mustafa, R. Nag, Eur. Phys. J. C **82**, 1006 (2022)
56. S. Das, N. Sarkar, A. Das, S.K. Pal, Eur. Phys. J. C **84**, 817 (2024)
57. S. Das, M. Govender, R.S. Bogadi, Eur. Phys. J. C **84**, 13 (2024)
58. P. Rej, R.S. Bogadi, M. Govender, Chin. J. Phys. **87**, 608–619 (2024)
59. S. Das, M. Govender, S. Aktar, Eur. Phys. J. C **84**, 1112 (2024)
60. S. Das, M. Govender, L. Baskey, Eur. Phys. J. C **85**, 1–10 (2025)
61. S.K. Pal, S. Das, A. Jangid, Braz. J. Phys. **55**, 30 (2025)
62. S. Das, S. Ray, A. Das, S.K. Pal, New Astron. **119**, 102393 (2025)
63. N. Pant, R.N. Mehta, M. Pant, Astrophys. Space Sci. **332**, 473 (2011)
64. Y.K. Gupta, S.K. Maurya, Astrophys. Space Sci. **332**, 155 (2011)
65. N. Pant, Astrophys. Space Sci. **331**, 633 (2011)
66. M. Sharif, T. Naseer, Chin. J. Phys. **73**, 179 (2021)
67. J.M. Sunzu, S.D. Maharaj, S. Ray, Astrophys. Space Sci. **352**, 719 (2014)
68. M.H. Murad, Astrophys. Space Sci. **20**, 361 (2016)

69. M. Sharif, S. Sadiq, Eur. Phys. J. C **78**, 410 (2018)
70. R.C. Tolman, Phys. Rev. **55**, 364 (1939)
71. J.R. Oppenheimer, G.M. Volkoff, Phys. Rev. **55**, 374 (1939)
72. C.W. Misner, D.H. Sharp, Phys. Rev. **136**, B571 (1964)
73. R.C. Tolman, Phys. Rev. **35**, 875 (1930)
74. M.S.R. Delgaty, K. Lake, Comput. Phys. Commun. **115**, 395 (1998)
75. B.V. Ivanov, Eur. Phys. J. C **77**, 738 (2017)
76. A. Giuliani, T. Rothman, Gen. Relativ. Gravit. **40**, 1427 (2008)
77. D. Naresh, J. Cosmol. Astropart. Phys. **04**, 035 (2020)
78. H.A. Buchdahl, Phys. Rev. **116**, 1027 (1959)
79. B.V. Ivanov, Phys. Rev. D **65**, 104011 (2002)
80. D.G. Ravenhall, C.J. Pethick, Astrophys. J. **424**, 846 (1994)
81. H. Abreu, H. Hernández, L.A. Núñez, Class. Quantum Gravity **24**, 4631 (2007)
82. L. Herrera, Phys. Lett. A **165**, 206 (1992)
83. B.K. Harrison, K.S. Thorne, M. Wakano, J.A. Wheeler, *Gravitational Theory and Gravitational Collapse* (University of Chicago Press, Chicago, 1965)
84. Y.B. Zeldovich, I.D. Novikov, *Relativistic Astrophysics Vol. 1: Stars and Relativity* (University of Chicago Press, Chicago, 1971)
85. H. Heintzmann, W. Hillebrandt, Astron. Astrophys. **38**, 51 (1975)
86. R. Chan, L. Herrera, N.O. Santos, Mon. Not. R. Astron. Soc. **265**, 533 (1993)
87. F. de Felice, Y.Q. Yu, J. Fang, Mon. Not. R. Astron. Soc. **277**, L17 (1995)
88. M.C. Durgapal, R.S. Fuloria, Gen. Relativ. Gravit. **17**, 671 (1985)
89. T. Gangopadhyay et al., Mon. Not. R. Astron. Soc. **431**, 3216 (2013)
90. P.B. Demorest, Nature **467**, 1081 (2010)
91. P.C.C. Freire et al., Mon. Not. R. Astron. Soc. **412**, 2763 (2011)
92. M.L. Rawls et al., Astrophys. J. **730**, 25 (2011)
93. S. Das, K. Chakraborty, F. Rahaman, S. Majumder, Eur. Phys. J. C **84**, 527 (2024)